Nucleic Acids Research, 2025, **53**, gkaf081
https://doi.org/10.1093/nar/gkaf081
Advance access publication date: 13 February 2025
Genome integrity, repair and replication

Multifaceted roles of H2B mono-ubiquitylation in D-loop metabolism during homologous recombination repair

Shih-Hsun Hung [1], **Yuan Liang** [1], **Wolf-Dietrich Heyer** [1,2,*]

[1]Department of Microbiology and Molecular Genetics, University of California, Davis, One Shields Ave, Davis, CA 95616, United States
[2]Department of Molecular and Cellular Biology, University of California, Davis, One Shields Ave, Davis, CA 95616, United States
[*]To whom correspondence should be addressed. Tel: +1 530 752 3001; Email: wdheyer@ucdavis.edu

Abstract

Repairing DNA double-strand breaks is crucial for maintaining genome integrity, which occurs primarily through homologous recombination (HR) in *Saccharomyces cerevisiae*. Nucleosomes, composed of DNA wrapped around a histone octamer, present a natural barrier to end resection to initiate HR, but the impact on the downstream HR steps of homology search, DNA strand invasion, and repair synthesis remain to be determined. Displacement loops (D-loops) play a pivotal role in HR, yet the influence of chromatin dynamics on D-loop metabolism remains unclear. Using the physical D-loop capture and D-loop extension (DLE) assays to track HR intermediates, we employed genetic analysis to reveal that H2B mono-ubiquitylation (H2Bubi) affects multiple steps during HR repair. We infer that H2Bubi modulates chromatin structure, not only promoting histone degradation for nascent D-loop formation but also stabilizing extended D-loops through nucleosome assembly. Furthermore, H2Bubi regulates DNA resection via Rad9 recruitment to suppress a feedback control mechanism that dampens D-loop formation and DLE at hyper-resected ends. Through physical and genetic assays to determine repair outcomes, we demonstrate that H2Bubi plays a crucial role in preventing break-induced replication and thus promoting genomic stability.

Graphical abstract

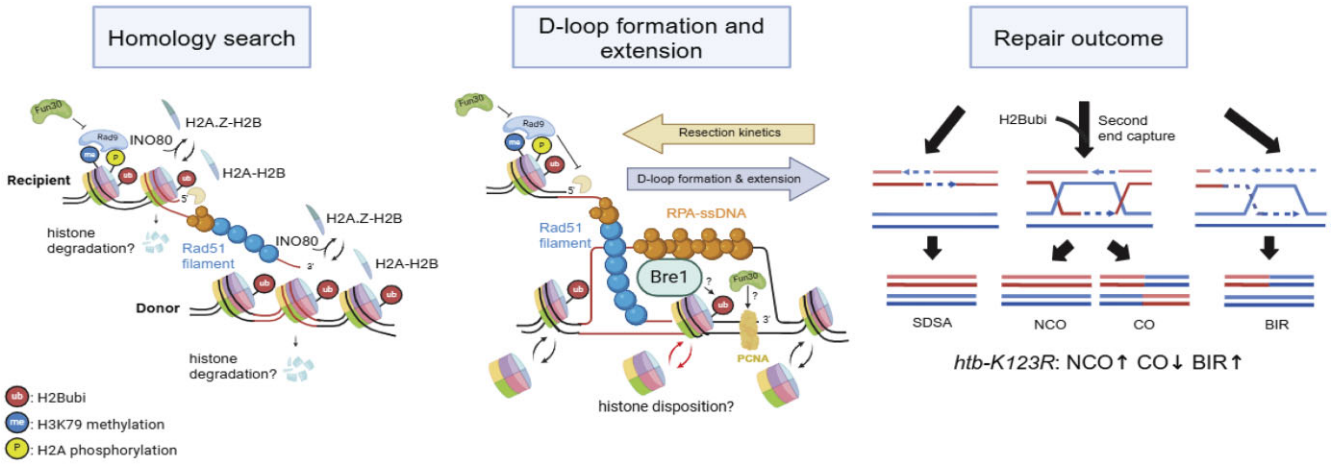

Introduction

Homologous recombination (HR) repair stands as a primary mechanism for resolving DNA double-strand breaks (DSBs) in *Saccharomyces cerevisiae*. During this process, the break termini undergo resection, leading to the formation of 3′ single-stranded DNA (ssDNA) tails, a crucial step in committing the DNA break to repair via HR [1, 2]. The recombinase protein Rad51 assembles onto the ssDNA to form the Rad51–ssDNA presynaptic filament, which is capable of searching for homology and invading homologous DNA, ultimately forming a DNA joint molecule termed the displacement loop (D-loop) [3]. DNA synthesis subsequently commences from the 3′ end of the invading strand, and the extended D-loop undergoes resolution through one of several sub-pathways to restore the integrity of the damaged chromosome, including synthesis-dependent strand annealing, double-strand break repair (DSBR) involving double Holliday junction formation, and break-induced replication (BIR) [4].

Two steps of HR undergo reversal and exist in a dynamic balance between forward and backward reactions [5, 6]: the

Received: September 12, 2024. **Revised:** January 21, 2025. **Editorial Decision:** January 22, 2025. **Accepted:** January 29, 2025

Rad51–ssDNA filament and the nascent D-loop. The formation of the Rad51–ssDNA filament requires the assistance of mediator proteins, while the Srs2 helicase/translocase disrupts the Rad51–ssDNA filament [7–16]. Additionally, the Sgs1–Top3–Rmi1 (STR) complex is involved in the disruption of the nascent D-loop [17–21]. Both Srs2 and Mph1 participate in the disruption of extended D-loops [19, 22–24]. Chromatin structure has been conceptualized as a barrier to repair that requires lifting and subsequent restoration [25]. Chromatin regulators have been shown to affect HR repair, especially end resection [26–36]. However, understanding of how chromatin regulators influence the kinetics of D-loop metabolism has been limited due to the absence of assays capable detecting nascent and extended D-loops during DNA repair in mitotically growing cells. Using a proximity ligation approach, this gap in the toolbox to study HR intermediates has been closed by the development of the D-loop capture (DLC) and D-loop extension (DLE) assays [19, 37]. This progress allowed to define two pathways of D-loop disruption, one involving the STR complex, likely favoring nascent D-loops, and one involving Srs2 involving extended, possibly longer D-loops [19]. Interestingly, the STR complex acts epistatically to Mph1, which is also capable of disrupting extended D-loops [19, 24]. Unlike other polymerase chain reaction (PCR)-based approaches to study DLE, which measure the double-stranded DNA (dsDNA) repair product [38, 39], the DLE assay allows to track the extension intermediate before conversion to double-stranded DNA (dsDNA) product [37]. Collectively, these advances provide avenues for studying D-loop metabolism within the context of chromatin.

In eukaryotes, DNA intricately wraps around histones to form nucleosomes. Thus, dynamic alterations in chromatin structure during HR repair can profoundly affect DNA resection, the subsequent homology search, followed by D-loop formation, and DLE. Chromatin structure is regulated through several mechanisms: histone modification, non-histone proteins, histone variants, histone chaperones, and ATP-dependent chromatin-remodeling enzymes [29]. In eukaryotic DNA replication, nucleosome disruption ahead of the replication fork and subsequent reassembly behind are essential processes [40]. During DLE, which resembles lagging strand DNA replication, the involvement of the DNA replication machinery including DNA polymerase delta, proliferating cell nuclear antigen (PCNA), and replication factor C (RFC) is necessary [38, 41–46]. However, whether nucleosomes are assembled into the three-strand stage of the D-loop remains an open question. Histone chaperones such as Asf1 and CAF-1 play crucial roles in regulating chromatin replication [47, 48]. They have also been reported to stabilize D-loops at stalled replication forks, ensuring replication restart in fission yeast [49, 50]. Moreover, nucleosome assembly at D-loops was inferred from studies of the HR-effect of human ATRX [51].

H2B mono-ubiquitylation at lysine 123 (H2Bubi) has a profound impact on chromatin structure interfering with chromatin compaction resulting in an open and accessible conformation [52]. Rad6, in cooperation with the E3 enzyme Bre1, plays a pivotal role in regulating H2Bubi in *S. cerevisiae*. H2Bubi has been associated with DSB repair through relaxing chromatin structure, as observed in studies conducted in both *S. cerevisiae* and human cell lines [53–58]. H2Bubi is reported to affect H3 methylation through Dot1-mediated H3K79 and Set1-mediated H3K4 methylation [59]. However, previous studies suggest that the HR repair function of H2Bubi is independent of H3K4 or H3K79 methylation [55]. Moreover, H2Bubi helps avoid hyper-resection by permitting Dot1-dependent H3K79 methylation for Rad9 recruitment, which is known to limit excessive resection [52, 55, 60]. Despite this, the role of H2Bubi in fine-tuning chromatin structure for DSB repair presents a paradox: it enhances accessibility for repair while simultaneously maintaining Rad9 chromatin binding to restrict excessive DNA end resection, thereby limiting the availability of ssDNA necessary for strand invasion. Investigating how H2Bubi affects DNA resection and D-loop metabolism should elucidate the molecular mechanisms underlying the complex role of H2Bubi in HR repair.

Here, we unveil the multifaceted roles of H2Bubi in D-loop metabolism and its effect on DSB repair pathway usage in *S. cerevisiae*. Through epistasis analysis using the DLC and DLE assays to determine D-loop levels and their extension, we reveal that H2Bubi modulates chromatin structure, not only promoting histone degradation for nascent D-loop formation but also stabilizing extended D-loops through nucleosome assembly, as inferred from published mutant phenotypes [56, 61]. Furthermore, H2Bubi regulates DNA resection via Rad9 recruitment, suppressing a feedback control mechanism that dampens D-loop formation and DLE. Through physical and genetic assays aimed at studying repair outcomes, we demonstrate that H2Bubi plays a crucial role in preventing BIR, a sub-pathway of DNA DSBR known to culminate in genomic instability.

Materials and methods

Yeast strains and growth conditions

The yeast strains and their genotypes (W303 *RAD5* background) utilized in this study are listed in Supplementary Table S3. Gene disruptions were achieved by replacing the indicated gene using a PCR-based strategy [62]. The *htbKR* strain was constructed by PCR amplifying a DNA segment containing the *HTB2* lysine-to-arginine point mutation (AAA to AGA) and the downstream selection marker (*HIS3*) from a yeast strain obtained from Dr Cheng-Fu Kao using the HTB2-C (GACACTGGTATTTCCCAGAAGTCTA) and HTB2-D (ATTTAGGTTCACTACACGAGCATTC) primers. Genomic DNA from histidine prototrophic transformants was sent for Sanger sequencing to confirm the presence of the *htb2-K123R* mutation. Subsequently, a DNA segment containing the *HTB1* lysine-to-arginine point mutation (AAG to AGG), and the downstream selection marker (*NatMX*) was PCR-amplified using the HTB1-C (CCATGTCTATCTTGAACTCTTTCGT) and HTB1-D (GGCTCGTGTGAACAATACTAGATTT) primers. This segment was transformed into the *htb2-K123R-HIS3* strain, resulting in the *htb1-K123R-natMX htb2-K123R-HIS3* (*htb-K123R*) strain, which specifically and completely abolishes H2Bubi. All yeast cells were cultured in YP medium (1% yeast extract, 2% peptone) supplemented with 2% (v/v) dextrose. For DLC/DLE assays, cells were initially grown in YPD medium (1% yeast extract, 2% peptone, 2% dextrose), then diluted and switched to YEP-lactate medium (1% yeast extract, 2% peptone, 2% lactate). For haploid endpoint assays, cells were grown in YEP-lactate medium before adding 2% galactose for *GAL-HO* induction. For diploid endpoint assays, cells were cultured in YPR medium (1% yeast extract, 2% peptone, 2% raf-

finose) before adding 2% galactose for *GAL-ISCEI* induction. All analyses were conducted during the log phase of growth at 30°C.

DLC and DLE assays

For DLC experiments, all strains were in the W303 *RAD5* background. They contain a copy of the GAL1/10-driven HO endonuclease gene at the *TRP1* locus on chromosome IV (Chr. IV). A point mutation inactivates the HO cut site at the mating-type locus (MAT) on Chr. III (*MATa-inc*). The DSB-inducible construct contains the 117-bp HO cut site, a 2086-bp-long homology A sequence (+4 to + 2090 of the LYS2 gene), and a 327-bp fragment of the PhiX174 genome flanked by multiple restriction sites. The DLC and DLE assays were conducted following established protocols with slight adjustments [19, 37, 63]. Specifically, zymolyase-lysed cells were immediately subjected to restriction digestion, ligation, and DNA purification steps following hybridization with oligonucleotides. The control experiments monitoring DSB formation, ligation efficiency, and a normalization locus are shown in Supplementary Figs S1–S5.

Determination of BIR frequency

BIR frequency determination followed the method outlined in [38]. In brief, cells were cultivated to exponential phase in YEP-lactate medium and then plated on YPD plates. After 3 days, colonies were counted and subsequently replicated onto synthetic complete medium lacking lysine (*LYS2* drop-out) plates or YPD plates containing geneticin (G418). Cell viability post-HO induction was calculated by dividing the number of colonies on YP galactose plates by those on YP glucose plates. The percentage of cells repairing via BIR was determined by dividing the number of cells on *LYS2* drop-out plates by the number on YP galactose plates, normalized to the number on YPD. BIR frequencies were determined three times for each strain.

Detection of BIR products formation

Cells were cultured in YEP-lactate medium, followed by the addition of 2% galactose to induce HO endonuclease expression. Genomic DNA (25 ng) was then subjected to PCR amplification using Phusion High-Fidelity DNA Polymerase with the following cycling conditions: initial denaturation at 98°C for 30 s, followed by 25 cycles of denaturation at 98°C for 10 s, and annealing/extension at 72°C for 150 s in a 25 µl reaction volume. BIR product detection utilized P1 and P2 primers, while HO cut detection employed D1 and D2 primers. Normalization of P1-P2 and D1-D2 products was achieved using C1 and C2 primers, as described previously [38].

DNA end resection determined by qPCR-based assay

Resection assay was performed as described in [64]. Cells were cultured in YEP-lactate medium and induced with 2% galactose. Genomic DNA (150 ng) was collected at 0-, 2-, and 4-h timepoints and digested with 10 units of *Alu*I at 37°C for 3 h. Subsequently, the digested DNA samples or mock digests were diluted in ice-cold ddH_2O and kept on ice for quantitative PCR (qPCR) analysis. Primers flanking the *Alu*I cutting site and located 1- and 5-kb away from the HO cut site were used to quantify end resection. A control primer pair targeting a region on *ARG4* lacking the *Alu*I site was used for normalization. qPCR was conducted using Light Cycler 480 SYBR Green I Master with the Light Cycler 480 System (Roche), as per following program: 95°C for 15 s, 61°C for 12 s, 72°C for 15 s, and repeated for 50 cycles. Triplicate reactions were performed for all primer pairs, and the average threshold cycle (Ct) value was calculated for each sample. The percentage of ssDNA present at each timepoint was determined using the formula described in [64].

Recombination outcome determined by haploid endpoint assay

The haploid yeast strain utilized for the ectopic recombination assay was previously detailed [65]. Plating efficiency (PE) was calculated by dividing the count of colonies from YP galactose plates by those from YP glucose plates. The distribution of crossover (CO) products was assessed via Southern blot hybridization, employing a *URA3* probe on *Apa*LI-*Pvu*II-digested genomic DNA, as outlined in [66].

Recombination outcome determined by diploid endpoint assay

The diploid yeast strain utilized for the ectopic recombination assay was previously described [67]. Cells were cultured in YPR medium until reaching the logarithmic phase, following which 2% galactose was added to induce *I-Sce*1 expression for 1.5–3 h, depending on the growth rate of the wild type (WT) and each mutant. Subsequently, cells were plated on YPD and allowed to grow for 2 days. YPD plates were then replica plated onto YPD with hygromycin B (200 µg/ml), YPD with nourseothricin (Nat; 67 µg/ml, clonNat), and SC (-Ura/-Met) plates to determine recombination outcomes and ensure proper chromosome segregation, respectively. Notably, the YPD plates were also replica plated onto re-induction (SC-Ade medium containing 2% raffinose and 1% galactose) plates to confirm that red colonies and the red halves of sector colonies were genuine long-tract gene conversions. Any red colonies that turned white after replica plating onto re-induction plates were not counted, as this indicated that not both DSB sites were cut during galactose induction in liquid culture. Statistical significance for the number of recombination events between given strains was calculated using Student's *t*-test. Independent inductions were performed at least two times for each strain.

Western blot

Yeast cell lysates were prepared using the trichloroacetic acid (TCA) method. Briefly, equivalent numbers of cells (4×10^7) were collected and resuspended in 500 µl of ddH_2O. Then, 75 µl of ice-cold NaOH/beta-mercaptoethanol (βME) solution (1.85 M/7.5% final) was added, followed by vortexing and incubation on ice for 15 min. After adding 75 µl of ice-cold 55% TCA and another round of vortexing, the lysates were incubated on ice for 10 min. The supernatant was completely removed after the final wash. Samples were suspended in 30 µl of high urea buffer [8 M urea, 200 mM Tris–HCl (pH 6.8), 1 mM ethylenediaminetetraacetic acid (EDTA), 5% (w/v) sodium dodecyl sulfate (SDS), 0.1% (w/v) bromophenol blue, 1.5% (w/v) dithiothreitol (DTT)] and denatured at 60°C for 10 min. Before analysis by sodium dodecyl sulfate–polyacrylamide gel electrophoresis, samples were briefly cen-

trifuged. The anti-H2B (active motif) antibody was utilized to detect histones H2B and H2Bubi.

Chromatin immunoprecipitation

Cells were cultured overnight in YEP-lactate medium (timepoint 0 h). A total of 2% galactose was added to induce HO endonuclease expression. Cells were collected at timepoints 4, 6, and 8 h post-DSB induction. Cells were fixed by adding fresh 37% paraformaldehyde (final concentration: 1%) for 20 min at room temperature with shaking. The fixation was quenched by adding glycine to a final concentration of 125 mM and incubating for 5 min at room temperature. Cells (1×10^9) were harvested and washed twice with cold 1× Tris-buffered saline (TBS). At this stage, cells can be stored at −80°C. The cell pellet was resuspended in 500 µl of chromatin immunoprecipitation (ChIP) lysis buffer [50 mM Tris–HCl (pH 7.5), 150 mM NaCl, 1 mM EDTA, 1% NP-40] supplemented with proteinase inhibitor (Pierce 88265) and 1 mM phenylmethylsulfonyl fluoride (PMSF). Cells were disrupted using 0.8 g glass beads at 4°C by vortexing on high for 3 cycles (15 min on, 1 min off). The lysate was carefully transferred to 1.5-ml tubes using gel loading tips. The lysate was centrifuged at 13 200 rpm for 15 min at 4°C and the supernatant was discarded. The chromatin pellet was resuspended in 300 µl of ice-cold ChIP lysis buffer. The sample was sonicated using a Bioruptor (Diagenode), repeating for four times [(30 s on, 30 s off, medium power) × 30 cycle] to shear the chromatin into 300- to 500-bp fragments. The sample was centrifuged at 13 200 rpm for 30 min at 4°C to remove cell debris. The equivalent of 10 OD units (2×10^8 cells) of solubilized chromatin was transferred to fresh 1.5-ml tubes and ChIP lysis buffer was added to bring the final volume to 500 µl. A total of 20 µl of chromatin was saved as the INPUT sample and stored at −80°C. The remaining 480 µl chromatin was used for immunoprecipitation (IP). Protein G sepharose (20 µl per ChIP) were washed three times with 500 µl of ChIP lysis buffer. To pre-bind the protein G sepharose with 2 µl of H2Bubi antibody (Novus Biologicals, NBP2-54770) samples were incubated at 4°C for 2 h. After pre-binding, the protein G sepharose were washed three times with 500 µl of ChIP lysis buffer. The chromatin was incubated with the pre-bound protein G sepharose at 4°C for 2 h with gentle mixing. The immunoprecipitates were washed for 5 min at room temperature in the following buffers: 1 ml ChIP lysis buffer, 1 ml wash buffer I [50 mM HEPES (pH 7.5), 0.5 M NaCl, 1 mM EDTA (pH 8), 0.1% SDS, 0.1% sodium deoxycholate], 1 ml wash buffer II [0.25 M LiCl, 0.5% NP-40, 0.5% sodium deoxycholate, 1 mM EDTA, 10 mM Tris–HCl (pH 7.5)], and 1 ml Tris-EDTA (TE) buffer. The immunoprecipitates were eluted by adding 250 µl of elution buffer [50 mM Tris–HCl (pH 7.5), 10 mM EDTA, 1% SDS] to both IP and INPUT tubes. The samples were incubated at 65°C for 20 min with shaking, followed by 10 min at room temperature on a nutator. The supernatant (IP material) was transferred into new tubes. Then, 5 µl of protease K (20 mg/ml) and 1.5 µl of 1 M $CaCl_2$ were added to both INPUT and IP samples, and incubated at 65°C overnight. The DNA was purified using a MinElute column (QIAGEN) and washed twice with Buffer PE (QIAGEN).

Quantitative real-time PCR

qPCR analysis was performed in accordance with the MIQE guidelines [68]. qPCR was conducted using the LightCycler® 480 SYBR Green I Master (Roche) and the primers listed in Supplementary Table S2, on a LightCycler® 480 System (Roche). SYBR Green dye incorporation into the PCR products was monitored in real-time after each cycle, allowing for the calculation of the Ct value, which defines the cycle number at which exponential amplification of PCR products begins. The PCR cycling conditions were as follows: 95°C for 15 s, 61°C for 12 s, 72°C for 15 s, and repeated for 50 cycles. The specificity of the amplified product was confirmed by determining its melting temperature. Fold changes for qPCR were calculated using the ΔΔCt method. Experiments were conducted with at least two biological replicates. Data were analyzed using the Light Cycler 480 Software 1.5.0.

Statistical analysis

Statistical analysis of DLC, DLE, DNA resection, and ChIP results for each mutant was compared with their respective paired mutants using a two-way ANOVA in Prism 10 (GraphPad Software). Experiments were conducted with at least two biological replicates. Additionally, the statistical analysis of genetic recombination outcomes for each mutant was compared with the WT and was conducted using unpaired Student's *t*-test.

Results

H2Bubi affects the kinetics of D-loops metabolism

To directly investigate the involvement of H2Bubi in the formation and extension of D-loops during HR repair, we employed the DLC and DLE assays [19, 37, 63], which are able to quantify the kinetics of nascent D-loop intermediate formation and DLE *in vivo* and distinguish themselves from other assays limited to measuring the final physical or genetic repair end products.

A site-specific DSB induced by HO endonuclease on Chr. V leads to homology search and DNA strand invasion of a 2-kb homologous donor sequence on Chr. II. Two *EcoR*1 sites were used for proximity ligation (Fig. 1B). After *GAL-HO* induction and DNA strand invasion at the donor site, *in vivo* interstrand DNA cross-linking by psoralen covalently links the heteroduplex DNA (hDNA) within the D-loop, preserving it during subsequent steps. A long complementary oligonucleotide is utilized to restore the restriction site that was ablated by DNA end resection. Subsequently, following restriction site restoration and digestion, the cross-linked hDNA, held together by psoralen, is preferentially ligated during the proximity ligation reaction under dilute conditions. The resulting unique chimeric ligation products are quantified by qPCR using a pair of specific primers, and this PCR product is referred to as the DLC signal (Fig. 1A). Extended D-loops were quantified using a similar proximity ligation approach to examine DLE to the downstream 396-bp *Hind*III site in the absence of psoralen cross-linking (Fig. 1E). Two long complementary oligonucleotides are used to restore the restriction sites. One serves to restore the restriction site ablated by DNA end resection, while the other is used to restore the *Hind*III site located 396-bp downstream of the invading 3′-OH end in the ssDNA extension intermediate in unique sequence following the homologous donor sequence. Following restriction site restoration and digestion, proximity ligation is employed to ligate the extended invading strand into a stable circular form of DNA molecule. The resulting unique chimera is quantified by

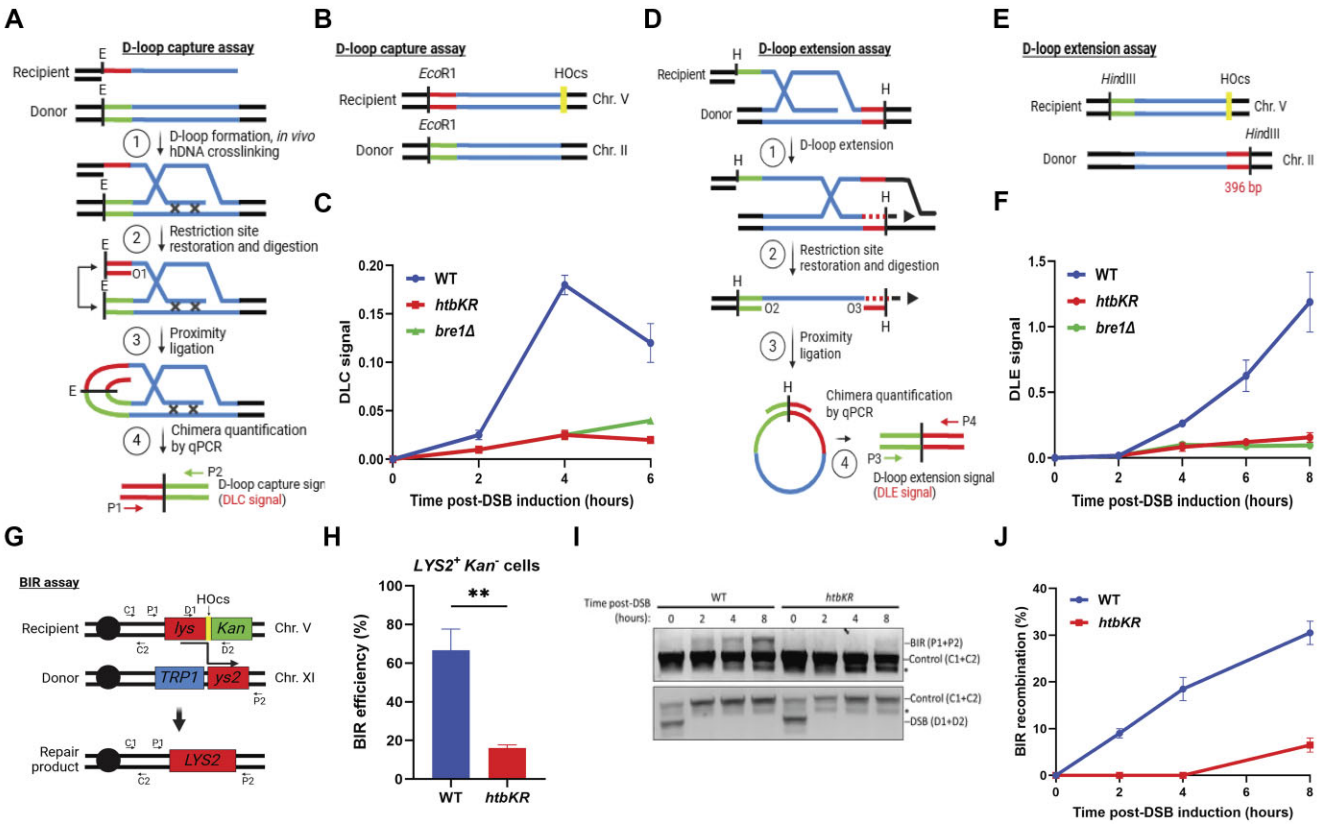

Figure 1. H2Bubi affects D-loop metabolism. (**A**) Schematic representation illustrating the rationale behind the DLC assay (see text for details). (**B**) Schematic representation depicting the construct of the DLC-assay strain. (**C**) Quantification of the DLC signal from the specified strains obtained at various timepoints following HO induction. Error bars, SEM ($n = 2$). (**D**) Schematic representation illustrating the rationale behind the DLE assay (refer to the text for details). (**E**) Schematic representation depicting the construct of the DLE-assay strain. (**F**) Analysis of the DLE signal from the specified strains was conducted at various timepoints following HO induction. Error bars, SEM ($n \geq 2$). (**G**) Schematic representation illustrating the construct for the BIR assay (see text for details). (**H**) BIR efficiency was determined by counting colony formation on YP-Gal [ensure that colonies are viable on LYS drop-out (*LYS2+*) and sensitive to geneticin (*Kan−*)] divided by YP-Glu for each of the indicated strains across three independent trials. Error bars, SEM ($n = 3$). $^{**}P = .0014$. (**I**) Agarose gel analysis was conducted to assess PCR products from various primer sets, examining the kinetics of BIR product formation (P1 and P2), DNA loading control (C1 and C2), and DSB cleavage efficiency (D1 and D2) from the indicated strains at various timepoints following HO induction. (**J**) Plot illustrating the quantification of BIR products at each timepoint, as obtained from panel (I). Fig. 1A, B, D, E and G were created in BioRender.com.

qPCR using specific primers, and this PCR product is referred to as the DLE signal (Fig. 1D). The DLC and DLE assays contain a number of quantitative controls to ensure reproducible quantitation including monitoring the level of DSB formation, a normalization control (*ARG4* locus), as well as controlling for the intramolecular ligation efficiency by measuring the ligation of a circularized DNA fragment from Chr. VIII following *Eco*R1 digestion (DLC assay) and a circularized DNA fragment from Chr. XII following *Hind*III digestion (DLE assay) [19, 37, 63].

As anticipated from previous results [19, 37, 63], in WT cells, D-loop formation was observed around 2 h post-DSB induction, peaking at 4 h before slightly declining at 6 h due to DLE and D-loop migration (Fig. 1C). As expected, DLE exhibited slower kinetics, first detected after 4 h, and gradually increasing until 8 h (Fig. 1F). Nascent and extended D-loops could be investigated separately due to this 2-h difference [19, 37]. For this reason, we focused in the subsequent genetic pathway analysis on the 2-h timepoint for DLC assay to evaluate nascent D-loop levels and the 8-h timepoint for the DLE assay to assess DLE. We observed a significant decrease in the DLC and DLE signals at all timepoints upon deletion of *BRE1* (*bre1Δ*) or in the *htbKR* mutant [lacking mono-ubiquitylation of H2B on lysine (K) 123 due to an amino acid change to arginine (R)] (Fig. 1C and F). The DLC signal at 4 h post-DSB in the *bre1Δ* and *htbKR* mutants resembled the DLC signal at 2 h post-DSB in WT cells but with no significant increase thereafter. Additionally, the DLE signal was significantly depressed with essentially no increase after 4 h post-DSB induction in the *bre1Δ* and *htbKR* mutant cells. Control experiments showed similar level of DSB induction efficiency by HO endonuclease and consistent individual values for the DLC and DLE control experiments in WT, *bre1Δ*, and *htbKR* cells (Supplementary Fig. S1). These results suggest that H2Bubi promotes DNA strand invasion to form and/or maintain nascent and extended D-loops. While the defect in DLE could be a mere consequence of the defect in D-loop levels, additional genetic analysis presented below suggests that both defects reflect separate functions of H2Bubi in HR employing distinct mechanisms.

The DLE assay is designed to detect the extension intermediate of BIR, as the system does not provide homology on the other DSB end to make the DSB repairable. This design was implemented to avoid complications from cells that repaired the DSB and resumed growth [19, 37, 63]. To further investigate the impact of H2Bubi on the kinetics of repair prod-

uct formation, we used a well-characterized genetic and physical assay for BIR [38, 69]. The repair of an induced HO cut on Chr. V depends on the search for and invasion of homology on Chr. XI (Fig. 1G). Following DSB induction, successful homology-directed repair can only occur via BIR to restore a functional *LYS2* gene, as evidenced by colony growth on synthetic medium lacking lysine. The loss of the *KanMX* gene confirms that the DSB was repaired by BIR and not by non-homologous end joining (Fig. 1H). BIR efficiency was assessed by measuring colony formation after DSB induction (Fig. 1H), and BIR kinetics were evaluated by detecting the BIR repair intermediates/products via PCR (Fig. 1I and J).

We observed a significant decrease in BIR efficiency in the *htbKR* mutant (Fig. 1H). Furthermore, BIR kinetics in the *htbKR* mutant was markedly delayed, emerging only at 8 h post-DSB induction, compared with the WT cells, where BIR products appeared 2 h post-DSB induction and gradually increased over time (Fig. 1I and J). Timepoints later than 8 h are difficult to interpret, as cells resume growth after repair. The disparity in BIR kinetics between WT and *htbKR* mutants does not seem to stem from differences in HO induction efficiency, as evidenced by comparable cutting efficiencies at the HO cut site. Significantly, no band indicative of an intact HO cut site was detected 2-h post-HO induction in both WT and *htbKR* mutant, as revealed by PCR, indicating near 100% DSB induction (Fig. 1I). Collectively, these findings strongly suggest that H2Bubi affects the kinetics of D-loop metabolism.

D-loop disruption pathways counteract nascent D-loop formation in the absence of H2Bubi

To further elucidate the role of H2Bubi in the dynamic equilibrium of nascent D-loop formation and disruption, we measured the DLC signal at 2 h post-DSB induction. At this timepoint, DLE is very limited, allowing the determination of nascent D-loop levels [19, 37]. It has been reported that two distinct pathways, one STR- and Mph1-dependent and the other Srs2-dependent, target different D-loop species (Fig. 2A) [19]. We thus compared the DLC signal in *htbKR* mutant in combination with *SGS1* (*sgs1Δ*) or *SRS2* (*srs2Δ*) deletions. In line with our previous results [19], we observed that *sgs1Δ* or *srs2Δ* resulted in a significant two- to three-fold increase in DLC signal (Fig. 2B and C). In addition, we observed that the reduced level of DLC signal in the *htbKR* mutant was restored to WT levels when combined with the *SGS1* deletion, although it remained lower than in the *sgs1Δ* single mutant (Fig. 2B). Surprisingly, in the *srs2Δ htbKR* double mutant, the DLC signal was restored to a level similar to that of the *srs2Δ* single mutant (Fig. 2C).

To delve deeper into the epistatic relationship between H2Bubi and the D-loop disruption pathways, we disabled the function of the STR complex by overexpressing a catalytically inactive mutant *top3-Y356F* (*top3-cd*) in both the *srs2Δ* single mutant and *srs2Δ htbKR* double mutant backgrounds along with WT Top3 as a control. This approach to generate a double mutant context is necessary, as the *sgs1Δ srs2Δ* double mutant is synthetically lethal [70]. Our findings revealed a significant two-fold increase in the DLC signal when *top3-cd* was overexpressed in the *srs2Δ* mutant background, consistent with the previous conclusion that the Srs2- and STR-dependent pathways are separate [19]. No significant change was observed upon overexpression of either Top3 or *top3-cd* in the *srs2Δ htbKR* double mutant background (Fig. 2D).

Together, these results suggest that H2Bubi promotes nascent D-loop levels. Notably, the deficiency in nascent D-loop levels can be restored by eliminating STR- or Srs2-dependent D-loop disruption pathways [19], underscoring the critical role of the D-loop disruption pathways in monitoring nascent D-loop levels. Moreover, H2Bubi may preferentially promote longer D-loop formation, which was proposed to be the target of the Srs2-dependent pathway (Fig. 2E) [19]. It is possible that this D-loop species involves chromatinization that depends on H2Bubi. Alternatively, Rad51–ssDNA filament stabilized by *srs2Δ* may promote homology search thus compensate the nascent D-loop formation defect in the *htbKR* mutant. We consider this alternative to be less likely, as the Rad51 paralog complex Rad55–Rad57 effectively insulates Rad51–sDNA filaments against disruption by Srs2 during DSB repair and the *srs2* single mutant that not display a DSB repair defect as indicated its WT resistance to IR [71]. Besides D-loop disruption, STR is also involved in DSB resection [72], but we consider it less likely that this role is relevant in our experimental system. The *sgs1* single mutant shows normal resection kinetics during MAT switching and no MAT switching defect as well as no resection defect for an unrepairable DSB [73, 74]. The repair defect of the *sgs1* single mutants only becomes apparent when measuring resection kinetics at 10 and more kb from the DSB site, but was shown to be normal up to 3 kb [75]. Our experimental system involves only 2-kb homology and requires resection for homology search and strand invasion that is demonstrably WT in the *sgs1* single mutant. In sum, multiple factors may contribute to the observed suppression of the defect in D-loop levels caused by a defect in H2Bubi, but we interpret the roles of Sgs1 and Srs2 in D-loop disruption as the major reason for the recovery of D-loop levels in the respective double mutants.

H2Bubi is epistatic to H2A.Z and INO80 in promoting nascent D-loop formation

Checkpoint activation and the INO80 chromatin remodeling complex (INO80-C) were shown to trigger histone degradation through the recruitment of several ubiquitin ligases and the proteasome to damaged chromatin, resulting in reduced chromatin compaction and enhanced chromosome movement [56, 76–78]. We thus determined the DLC signal in mutants in two well-studied chromatin regulators, the INO80 complex (INO80-C) and the high-mobility group proteins *NHP6A/B*, which were previously described as having compacted and expanded chromatin, respectively [76] (Fig. 3A). We measured the DLC signal at 2 h, which represents nascent D-loops, as extension starts only later (Fig. 1C and F). Indeed, the deletion of the *INO80-C* subunit *ARP8* (*arp8Δ*) resulted in a five-fold reduction of the DLC signal compared with the WT, and no significant difference was observed between *arp8Δ*, *htbKR*, and *arp8Δ htbKR* mutants (Fig. 3B). In contrast, the reduced DLC signal in the *htbKR* mutant was restored to WT levels when combined with the *NHP6A/B* deletion (*nhp6ΔΔ*) mutant (Fig. 3C). This restoration is likely due to a 20% reduction in histone occupancy in the *nhp6ΔΔ* background [56, 77, 79], suggesting a role for H2Bubi in promoting nascent D-loop levels via the described histone degradation pathway after DNA damage. Our results are consistent with a previous study demonstrating that Rad6 and Bre1 are both recruited to chromatin upon DNA damage and contribute to recombina-

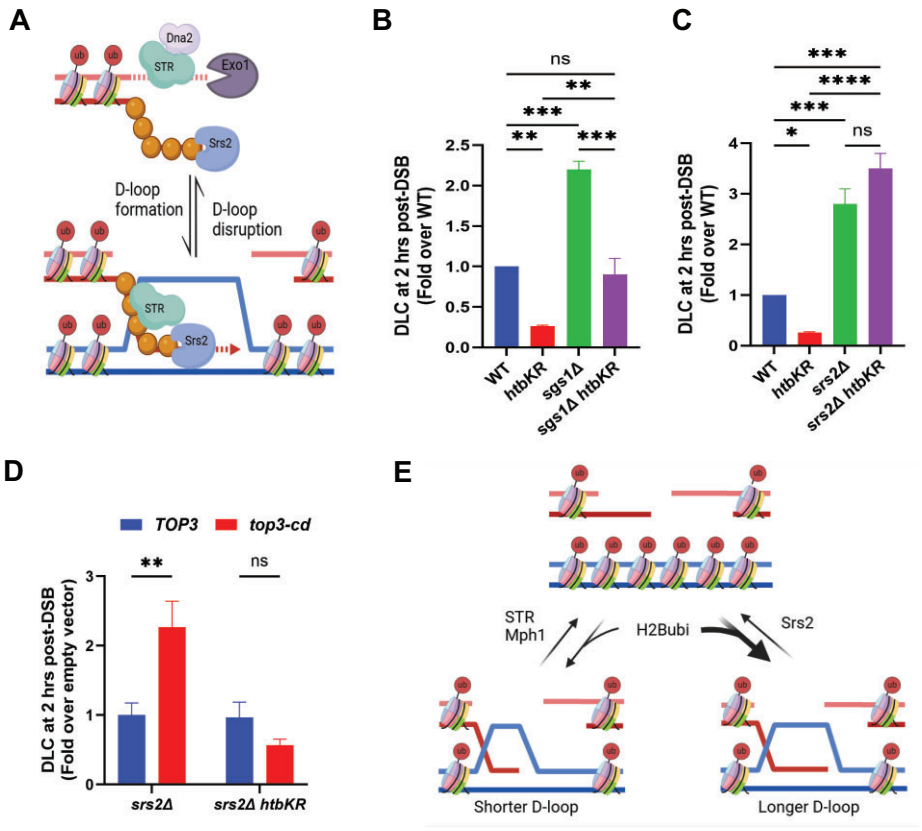

Figure 2. D-loop disruption pathways prohibit D-loop formation in the absence of H2Bubi. (**A**) HR repair begins with the invasion of a homologous duplex by a 3′ overhang formed through DNA end resection (STR-Dna2 or Exo1). The invasion of the 3′ end is monitored by the STR and Mph1 epistatic pathways, alongside the Srs2-dependent D-loop disruption pathway. (**B**) Quantification of the DLC signal in WT, *htbKR*, and *sgs1Δ* was examined individually and in double mutant combinations. Error bars, SEM ($n \geq 2$). $^{**}P = .0068$, $^{***}P = .0002$. (**C**) Quantification of the DLC signal in WT, *htbKR*, and *srs2Δ* was examined individually or in double mutant combinations. Error bars, SEM ($n \geq 2$). $^{*}P = .04$, $^{***}P = .0008$, $^{****}P = .0001$, ns: not significant. (**D**) Quantification of the DLC signal in the *htbKR* mutant, either with the absence of Srs2 or with the absence of both STR and Srs2-dependent D-loop disruption pathways. Error bars, SEM ($n = 3$). $^{**}P = .006$, ns: not significant. (**E**) H2Bubi may promote longer D-loop formation, as evidenced by the observation that blocking the Srs2-dependent pathway rescues more D-loop levels compared with blocking the STR pathway. Fig. 2A and E were created in BioRender.com.

tion by monitoring chromosome movement and the total level of repair products [56].

To further support the notion that H2Bubi affects HR through chromatin decompaction, we examined the histone chaperons CAF-1 and Asf1, which are involved in chromatin assembly through histone H3-H4 deposition [61] (Fig. 3D). We used a *cac1Δ* strain to disable CAF-1 and the *asf1Δ* mutant. Both exhibited a 1.5-fold increase in nascent D-loop level compared with WT cells (Fig. 3E and F), consistent with the role of Asf1 and CAF-1 in preventing unwanted recombination through the deposition of histone H3-H4 [80]. Additionally, deletions of *ASF1* or *CAF-1* have been reported to increase the rate of spontaneous gross chromosome rearrangements [81]. We observed that the reduced DLC signal in the *htbKR* mutant was significantly restored in combination with the *cac1Δ* or *asf1Δ* mutants (Fig. 3E and F). This further suggests that in the absence of H2Bubi, chromatin becomes more compacted due to the deficiency of the proteasome-dependent histone degradation pathway [56, 77, 79], leading to interference with nascent D-loop formation. Thus, reducing histone occupancy alleviates the defect.

The linker DNA serves to connect nucleosome core particles. Additionally, the complete nucleosome assembly may incorporate the linker histone H1, encoded by *HHO1* in *S. cerevisiae* [82]. This histone associates with the exterior of the core particle structure, particularly where the DNA enters and exits (Fig. 3G). It is believed that histone H1 plays a role in organizing higher order chromatin structure by facilitating chromatin condensation. Supporting this concept, research conducted in budding yeast has demonstrated that Hho1 restrains HR-mediated repair [56, 83]. We conducted an analysis involving *hho1Δ* mutants in conjunction with *htbKR* in the DLC assay. The *hho1Δ* mutants exhibited a 1.5-fold increase in nascent D-loops compared with WT cells (Fig. 3H). The *hho1Δ htbKR* double mutant showed no significant difference compared with the *htbKR* mutant alone, indicating that H2Bubi likely functions upstream of Hho1 in the proteasome-dependent degradation of both core and linker histones [56] (Fig. 3H).

Both the INO80 and SWR complexes are recruited to site of DSBs and engage in the exchange of H2A–H2B dimers, consequently modulating the presence of the H2A variant, H2A.Z [84–86], which is encoded by *HTZ1* in *S. cerevisiae* (Fig. 3I). To explore the impact of H2A.Z occupancy on nascent D-loop formation, we examined the DLC signal in *arp8Δ* (INO80-C), *swr1Δ* (SWR-C), and *htz1Δ* (H2A.Z) strains. Intriguingly, the *arp8Δ* mutant, characterized by elevated H2A.Z occupancy, exhibited significantly lower DLC levels compared with

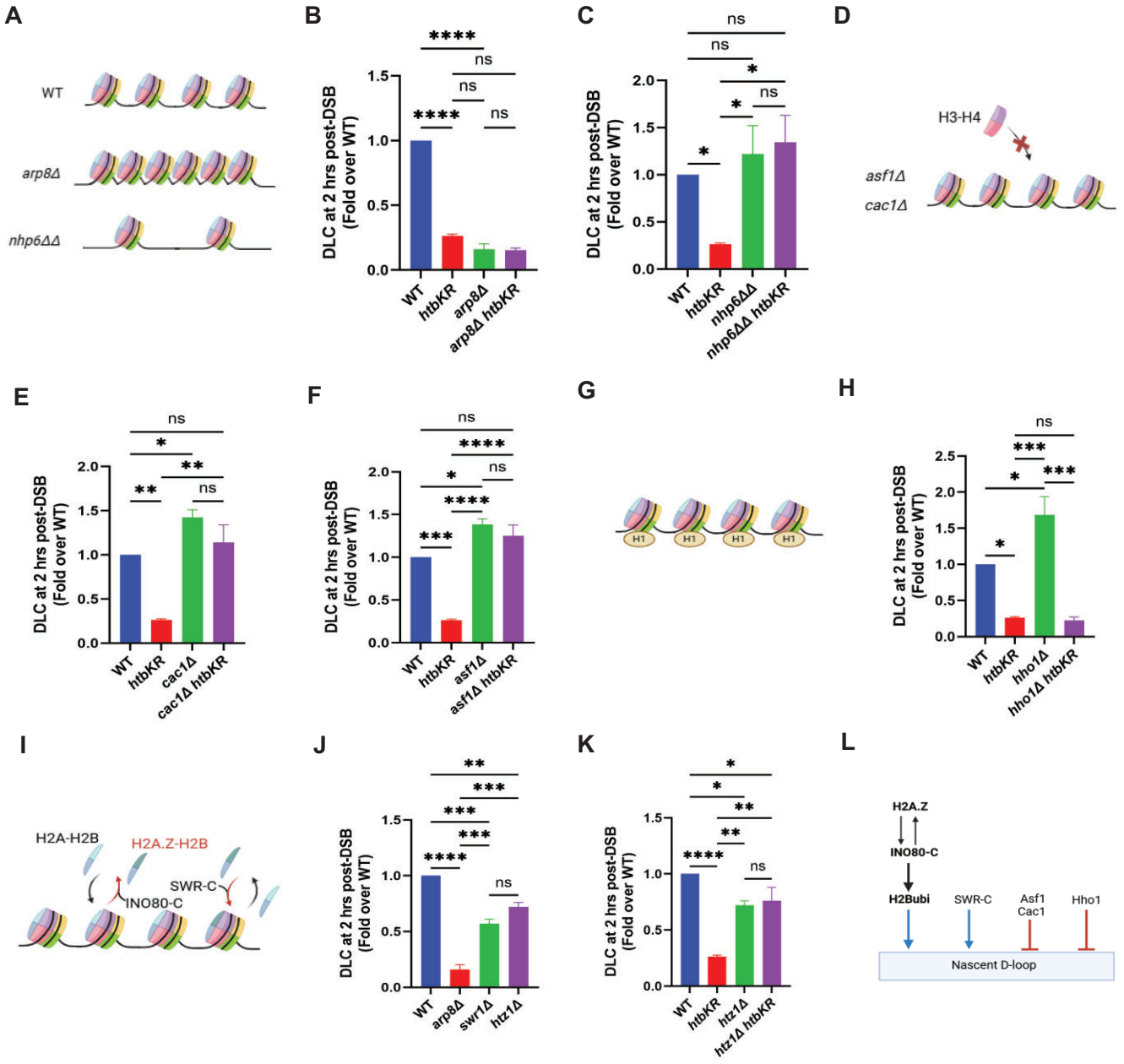

Figure 3. H2Bubi is epistatic to H2A.Z and INO80 in promoting nascent D-loop formation. (**A**) Schematic representation showing that *nhp6ΔΔ* cells exhibit reduced histone occupancy, while *arp8Δ* cells display more condensed chromatin. (**B**) DLC signal in WT, *htbKR*, *arp8Δ*, and *arp8Δ htbKR* strains. Error bars, SEM ($n = 3$). $^{****}P < .0001$, ns: not significant. (**C**) DLC signal in WT, *htbKR*, *nhp6ΔΔ*, and *nhp6ΔΔ htbKR* strains. Error bars, SEM ($n \geq 2$). $^{*}P < .03$, ns: not significant. (**D**) Asf1 and CAF-1 are histone chaperones responsible for depositing histone H3-H4 onto DNA. Lack of Asf1 or CAF-1 results in reduced histone occupancy. (**E**) DLC signal in WT, *htbKR*, *cac1Δ*, and *cac1Δ htbKR* strains. Error bars, SEM ($n \geq 2$). $^{*}P = .04$, $^{**}P < .0015$, ns: not significant. (**F**) DLC signal in WT, *htbKR*, *asf1Δ*, and *asf1Δ htbKR* strains. Error bars, SEM ($n \geq 2$). $^{*}P = .01$, $^{***}P = .0002$, $^{****}P < .0001$, ns: not significant. (**G**) Histone H1 is a linker histone that binds the outside of nucleosomes and modifies chromatin structure. (**H**) DLC signal in WT, *htbKR*, *hho1Δ*, and *hho1Δ htbKR* strains. Error bars, SEM ($n = 3$). $^{*}P < .02$, $^{***}P = .0002$, ns: not significant. (**I**) The INO80 and SWR complexes are chromatin remodelers responsible for facilitating histone dimer exchange. (**J**) DLC signal in WT, *arp8Δ*, *swr1Δ*, and *htz1Δ* strains. Error bars, SEM ($n = 2$). $^{**}P = .005$, $^{***}P < .0007$, $^{****}P < .0001$, ns: not significant. (**K**) DLC signal in WT, *htbKR*, *htz1Δ*, and *htz1Δ htbKR* strains. Error bars, SEM ($n \geq 2$). $^{*}P < .04$, $^{**}P < .002$, $^{****}P < .0001$, ns: not significant. (**L**) A schematic representation indicating that H2A.Z and INO80-C likely operate upstream of H2Bubi in regulating D-loop formation. SWR1-C promotes nascent D-loop formation. Hho1, Asf1, and Cac1 negatively regulate nascent D-loop formation. Fig. 3A, D, G, I, and L were created in BioRender.com.

both the *swr1Δ* mutant, which has reduced H2A.Z occupancy, and the *htz1Δ* mutant. However, the DLC signal in both the *swr1Δ* and *htz1Δ* single mutants was significantly reduced compared with WT, suggesting that both the deposition and removal of H2A.Z are important for nascent D-loop formation (Fig. 3J). A previous study demonstrated that H2A.Z recruits INO80-C to DSBs, where INO80-C subsequently removes H2A.Z during Rad51 filament formation [86]. Remarkably, we observed that the reduced DLC signal in the *htbKR* mutant was significantly restored in combination with the *htz1Δ* mutant (Fig. 3K). This finding suggests that H2A.Z, INO80, and H2Bubi likely function in the same pathway in the process of proteasome-dependent histone degradation [56] and facilitating Rad51 filament formation.

In summary, these findings suggest that H2A.Z, INO80-C, and H2Bubi promote nascent D-loop formation through a proteasome-dependent mechanism, as shown by the Gasser laboratory [56], that involves the degradation of core and linker histones and the formation of Rad51 filaments. Additionally, our data show that SWR1 promotes nascent D-loop formation, while Asf1, Cac1, and Hho1 act as negative regulators (Fig. 3L).

H2Bubi stabilizes extended D-loop

The regulatory influence of H2Bubi on D-loop metabolism, through nucleosome assembly and/or disassembly, could be intricate. It may impact not only the formation of nascent D-loops via histone degradation mechanisms [56] but also the disassembly of nucleosome ahead of the extending D-loop and/or the stabilization of extended D-loops through nucleosome assembly (Fig. 4A). Building upon the observation that compromising D-loop disruption factors and reducing histone occupancy can restore the nascent D-loop level to WT levels in the *htbKR* mutant (Figs 2 and 3), we further investigated these mutants using the DLE assay to measure the next step in HR, extension of the nascent D-loop [37]. We performed the DLE assay at 8 h post-DSB, as essentially all ends are extended at this timepoint in WT cells (Fig. 1F) [37].

We observe that the DLE signal of *sgs1Δ*, *srs2Δ*, *cac1Δ*, and *asf1Δ* single mutants exhibited no significant difference compared with WT cells at 8 h post-DSB (Fig. 4B, C, E, and F), suggesting that these mutants specifically affect the kinetics of nascent D-loop formation but have little or no effect on the kinetics of DLE and by inference on the absolute D-loop levels. The *sgs1Δ* and *srs2Δ* data are consistent with previous observations [37].

When comparing the DLE signal of *sgs1Δ htbKR* with *srs2Δ htbKR* to the *htbKR* single mutant, we observed that the DLE signal was more significantly restored in the *srs2Δ htbKR* compared with *htbKR* mutant, than in the *sgs1Δ htbKR* mutant compared with *htbKR* mutant (Fig. 4B and C). This observation aligns with the DLC assay results, which showed a faster kinetic of nascent D-loop formation in the *srs2Δ htbKR* mutant compared with the *sgs1Δ htbKR* mutant (Fig. 2B and C). Moreover, the faster nascent D-loop formation kinetics but limited DLE of the *srs2Δ htbKR* double mutant suggests that H2Bubi may have an additional function in extended D-loop progression and/or stabilization. Intriguingly, the *nhp6ΔΔ htbKR*, *cac1Δ htbKR*, and *asf1Δ htbKR* mutants exhibited no significant difference compared with the *htbKR* single mutant by DLE assay (Fig. 4D, E, and F). This suggests that H2Bubi may stabilize extended DLE through nucleosome assembly, while its role in nascent D-loop formation involves histone degradation mechanisms [56]. This could be mediated by recruitment of Rad6–Bre1 through its interaction with RPA which binds to the displaced strand of the D-loop [87, 88].

The *nhp6ΔΔ* mutant exhibits a 1.5-fold increase in extended D-loop compared with WT cells (Fig. 4D), while nascent D-loop levels remained largely unchanged (Fig. 3C) [37]. This suggests that reducing nucleosome occupancy through *nhp6ΔΔ* promotes DLE. Interestingly, the *htz1Δ* mutant displayed a 50% decrease in extended D-loop levels compared with the WT (Fig. 4G). Note that this effect was stronger than the 30% reduction in nascent D-loop levels (Fig. 3K), suggesting a possible function of H2A.Z in stabilizing extended D-loop. Furthermore, the *htz1Δ htbKR* double mutant showed no significant difference in DLE signal compared with the *htz1Δ* single mutant (Fig. 4G), suggesting that H2A.Z functions upstream of H2Bubi for control of DLE. This observation aligns with the DLC assay results, which showed a restored nascent D-loop level in the *htz1Δ htbKR* mutant (Fig. 3K).

Together, these results suggest that H2A.Z and H2Bubi are epistatic in stabilizing extended D-loops, likely by finely tuning nucleosome assembly and disassembly. Additionally, our data reveal a novel function of Nhp6A/B as negative regulators of DLE (Fig. 4H).

To monitor H2Bubi levels, we performed ChIP experiments in WT and *htbKR* cells, using three primer sets to measure H2Bubi levels at the donor site (Fig. 4I) and one primer set to assess H2Bubi levels at 5 kb from the break site (Supplementary Fig. S4C). In WT cells, we observed a significant increase in H2Bubi levels at the DLE regions (P2 and P3 primer sets) of the donor site (Fig. 4J) and at 5 kb from the break site (Supplementary Fig. S4D), but not at the other region of the donor site (P1) (Fig. 4J). In addition, no such increase was observed in *htbKR* cells (Fig. 4J and Supplementary Fig. S4D). These results further support a role of H2Bubi assembly at the donor site during DLE (Fig. 4A).

Excessive resection counteracts nascent D-loop formation

H2Bubi likely promotes nascent D-loop formation by facilitating histone degradation [56]. Next, we were curious whether H2Bubi also regulates D-loop metabolism by controlling DNA end resection through the recruitment of Rad9 [60, 89]. The recruitment of Rad9 is orchestrated by chromatin binding facilitated by H2A phosphorylation and Dot1-mediated H3K79 methylation, as well as Dpb11 binding through the 9–1–1 DNA checkpoint clamp (Fig. 5A) [90]. Importantly, in cells lacking H2Bubi, Rad9 recruitment to chromatin via H3K79 methylation is disrupted, while H2A phosphorylation and Dpb11 binding are preserved, thereby maintaining proficiency in checkpoint activation through the 9–1–1 clamp [60]. This scenario provides an opportunity to analyze the specific role of Rad9 in controlling resection during D-loop metabolism through analysis of the *htbKR* mutant.

Fun30, a chromatin remodeler, has been identified as a competitor of Rad9 for chromatin and Dpb11 binding [91–94] (Fig. 5A). Thus, we hypothesized that deletion of *FUN30* would lead to a deceleration of resection kinetics in the *htbKR* mutant. To test the hypothesis, we assessed resection kinetics using a well-established qPCR-based assay [64]. Primers were strategically designed to flank the *Alu*I cutting sites located

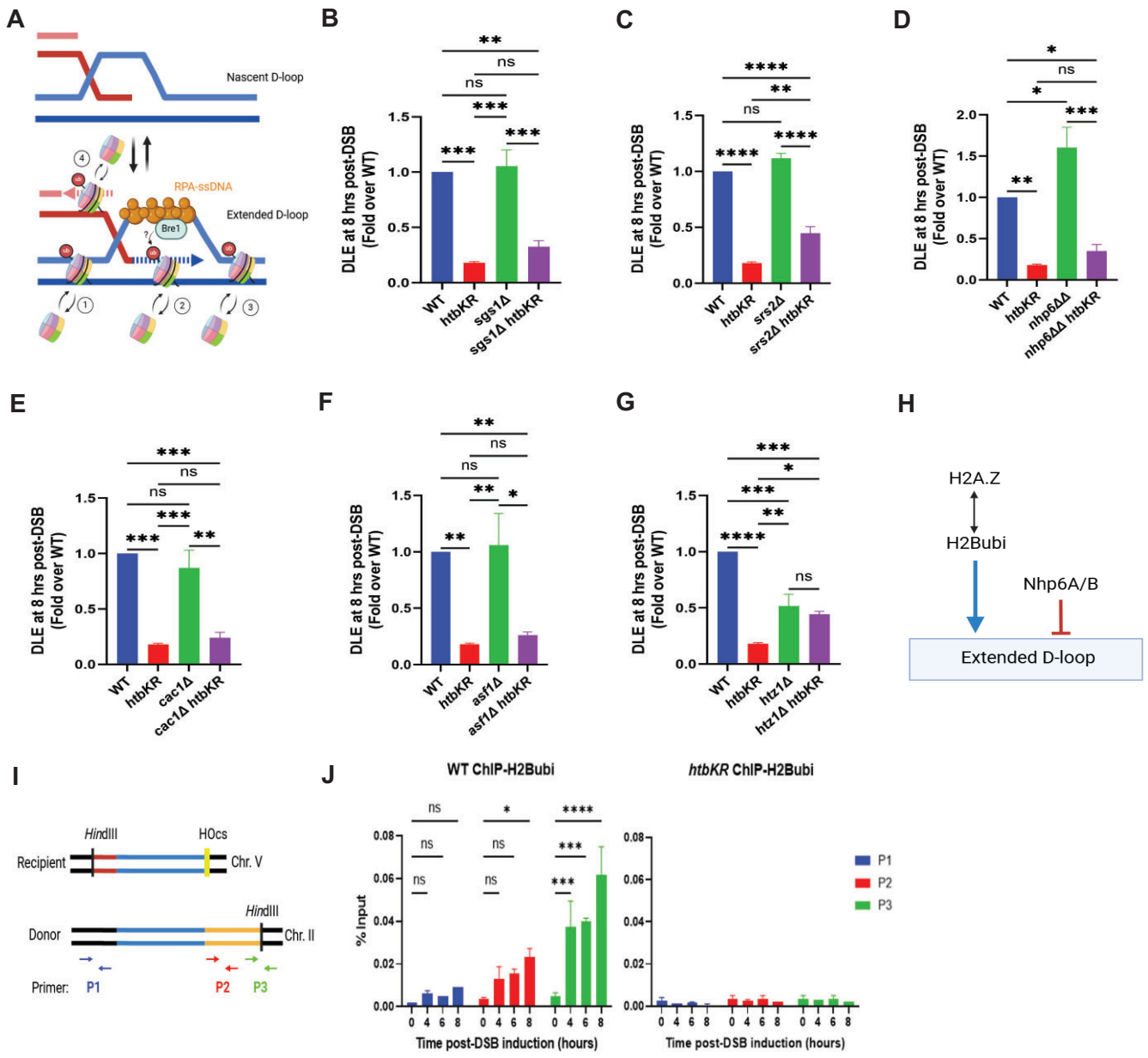

Figure 4. H2Bubi stabilizes extended D-loop. (**A**) An illustration depicting the process of D-loop formation and DLE within the context of chromatin. H2Bubi may stabilize the extended D-loop through nucleosome assembly and/or promote nucleosome disassembly ahead of the extended D-loop. Additionally, the E3 ligase Bre1, which is responsible for H2Bubi, has been reported to interact with Rpa [87], raising the possibility that H2Bubi is enriched at the D-loop. (**B**) Quantification of the DLE signal in WT, *htbKR*, *sgs1Δ*, and *sgs1Δ htbKR* strains. Error bars, SEM ($n = 3$). $^{**}P = .001$, $^{***}P < .0008$, ns: not significant. (**C**) Quantification of the DLE signal in WT, *htbKR*, *srs2Δ*, and *srs2Δ htbKR* strains. Error bars, SEM ($n = 3$). $^{**}P = .004$, $^{****}P < .0001$, ns: not significant. (**D**) Quantification of the DLE signal in WT, *htbKR*, *nhp6ΔΔ*, and *nhp6ΔΔ htbKR* strains. Error bars, SEM ($n \geq 2$). $^{*}P < .02$, $^{**}P = .002$, $^{***}P < .0006$, ns: not significant. (**E**) Quantification of the DLE signal in WT, *htbKR*, *cac1Δ*, and *cac1Δ htbKR* strains. Error bars, SEM ($n \geq 2$). $^{**}P = .003$, $^{***}P < .001$, ns: not significant. (**F**) Quantification of the DLE signal in WT, *htbKR*, *asf1Δ*, and *asf1Δ htbKR* strains. Error bars, SEM ($n \geq 2$). $^{*}P = .01$, $^{**}P < .004$, ns: not significant. (**G**) Quantification of the DLE signal in WT, *htbKR*, *htz1Δ*, and *htz1Δ htbKR* strains. Error bars, SEM ($n \geq 2$). $^{*}P = .01$, $^{**}P = .005$, $^{***}P < .0006$, $^{****}P < .0001$, ns: not significant. (**H**) A schematic representation indicating that H2Bubi and H2A.Z promote DLE, while Nhp6A/B suppresses it. (**I**) Schematic representation illustrating the location of the primer sets used in the qPCR assay to monitor H2Bubi at the donor site. (**J**) Quantification of H2Bubi levels at the donor site in WT and *htbKR* strains. Error bars, SEM ($n = 2$). $^{*}P = .02$, $^{***}P < .0005$, $^{****}P < .0001$, ns: not significant. Fig. 4A, H, and I were created in BioRender.com.

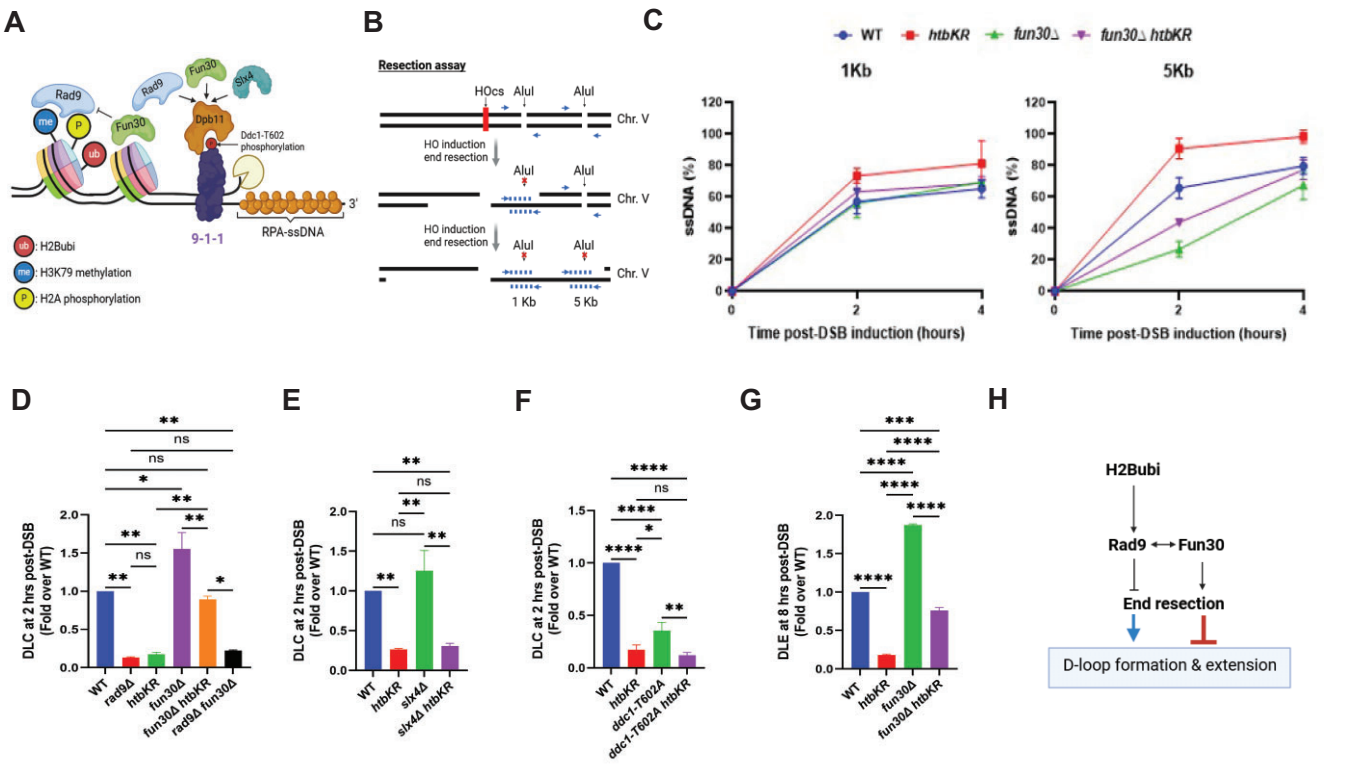

Figure 5. Excessive resection counteracts nascent D-loop formation and DLE. (**A**) Model illustrating the role of H2Bubi in regulating DNA end resection through Rad9 recruitment. Rad9 can be recruited to chromatin via H3K79 methylation and H2A phosphorylation, as well as through the Dpb11 9–1–1 axis. Fun30 competes with Rad9 for chromatin binding and Dpb11 9–1–1 binding. Slx4 specifically affects Rad9 binding to the Dpb11 9–1–1 axis. (**B**) Schematic representation illustrating the qPCR assay for monitoring DNA end resection. (**C**) Plot showing the percent of ssDNA among HO cut DNA at each timepoint by qPCR analysis. Error bars, SEM ($n = 3$). (**D**) DLC signal in WT, *rad9Δ*, *htbKR*, *fun30Δ*, *fun30Δ htbKR*, and *rad9Δ fun30Δ* strains. Error bars, SEM ($n \geq 2$). $^{*}P < .02$, $^{**}P < .008$, ns: not significant. (**E**) DLC signal in WT, *htbKR*, *slx4Δ*, and *slx4Δ htbKR* strains. Error bars, SEM ($n \geq 2$). $^{**}P < .009$, ns: not significant. (**F**) DLC signal in WT, *htbKR*, *ddc1-T602A*, and *ddc1-T602A htbKR* strains. Error bars, SEM ($n \geq 2$). $^{*}P = .01$, $^{**}P = .006$, $^{****}P < .0001$, ns: not significant. (**G**) Quantification of the DLE signal in WT, *htbKR*, *fun30Δ*, and *fun30Δ htbKR* strains. Error bars, SEM ($n \geq 2$). $^{***}P = .0003$, $^{****}P < .0001$, ns: not significant. (**H**) Schematic representation showing that H2Bubi affects nascent D-loop formation and DLE by coordinating DNA end resection through Rad9 chromatin recruitment. Fig. 5A, B, and H were created in BioRender.com.

1 and 5 kb from the HO cut site. Since *Alu*I cannot cut ssDNA, this design allows for the amplification of PCR products from the ssDNA region generated by resection (Fig. 5B). Indeed, we observed hyper-resection kinetics in the *htbKR* mutant and slowed resection kinetic in the *fun30Δ* mutant, consistent with earlier findings [55, 91] (Fig. 5C). Moreover, we noted a significant reduction in resection kinetics in the *fun30Δ htbKR* when compared with the *htbKR* single mutant (Fig. 5C). Control experiments using western blots showed that *fun30Δ* does not affect H2Bubi levels (Supplementary Fig. S5A).

To investigate whether resection kinetics impacts nascent D-loop formation, we compared the levels of nascent D-loop formation among WT, *rad9Δ*, *htbKR*, *fun30Δ*, *fun30Δ htbKR*, and *rad9Δ fun30Δ* using the DLC assay at the 2 h timepoint. Surprisingly, we observed that the *fun30Δ* strain, which exhibited slower resection kinetics, displayed increased nascent D-loop levels (Fig. 5D). Conversely, the *rad9Δ* and *htbKR* strain, characterized by faster resection kinetics, showed reduced nascent D-loop levels at 2 h (Fig. 5D), suggesting an inverse relationship between resection kinetics and nascent D-loop levels. Notably, *fun30Δ* rescued the reduced nascent D-loop levels in the *htbKR* mutant but not in the *rad9Δ* mutant, indicating that Fun30 primarily competes with Rad9 in controlling end resection (Fig. 5D). Consistent with this, a previous study found that *fun30Δ* does not slow down hyper-resection in the *rad9Δ* mutant [91]. Additionally, we observed that the reduced DLC signal in the *htbKR* mutant was restored to WT levels in the *htbKR nhp6ΔΔ* double mutant (Fig. 3C), but not in the *rad9Δ nhp6ΔΔ* double mutant (Supplementary Fig. S5B). This suggests that H2Bubi modulates chromatin structure for nascent D-loop formation, whereas Rad9 does not. Through examining Slx4, a protein known to compete with Rad9 for binding to Dpb11 but lacking influence on Rad9 chromatin binding [95, 96], we found that the *slx4Δ* mutation does not rescue the decreased nascent D-loop levels in the *htbKR* mutant (Fig. 5E). This finding lends support to the hypothesis that H2Bubi primarily impacts Rad9 chromatin binding rather than Dpb11 binding. To further support this notion, we disrupted the Mec1-dependent Ddc1 phosphorylation site (*ddc1-T602R*), which is crucial for the recruitment of Rad9, Slx4, and Fun30 to Dpb11 [94, 96–98]. This mutation failed to rescue the DLC defect observed in the *htbKR* mutant, indicating that H2Bubi operates independently of the Dpb11 9–1–1 axis in nascent D-loop formation (Fig. 5F).

Building on the observation that slowing down resection through *fun30Δ* can restore nascent D-loop levels to WT levels in the *htbKR* mutant (Fig. 5D), we further investigated these mutants using the DLE assay to measure the next step in HR—the extension of the nascent D-loop. The *fun30Δ* mu-

tant exhibits a two-fold increase in extended D-loop levels compared with WT cells (Fig. 5G), a more pronounced effect than the 1.5-fold increase observed in nascent D-loop levels (Fig. 5D). This suggests a novel role for Fun30 in negatively regulating DLE. Additionally, the DLE signal was partially restored in the *fun30Δ htbKR* double mutant compared with the single mutants *htbKR* and *fun30Δ* (Fig. 5G). This finding aligns with the DLC assay results, which showed restored nascent D-loop levels in the *fun30Δ htbKR* mutant (Fig. 5D), indicating that Fun30 acts epistatically to H2Bubi in controlling D-loop formation and DLE.

Taken together, these data suggest that excessive resection negatively feeds back on nascent D-loop formation and that H2Bubi plays a role in this process likely through regulating Rad9 chromatin binding (Fig. 5H).

H2Bubi affects DSB repair pathway usage and outcome

To explore the impact of H2Bubi on DSB repair pathway usage and outcomes, we used a previously described DSB-induced mitotic recombination assay. This assay monitors both reciprocal and nonreciprocal exchange end products in diploid cells monitoring CO and non-crossover (NCO) outcomes as well as BIR and chromosome loss along with additional events leading to loss of heterozygosity [67]. In this system, an *I-Sce1* cut site is introduced within the *ADE2* locus (*ade2-I*) on one Chr. XV, while the other homolog carries an inactive allele of *ADE2* (*ade2-n*). The repair outcome is assessed using two antibiotic resistance genes, *HPH* and *NAT*. Additionally, *MET22* and *URA3* were employed to trace chromosome loss events (Fig. 6A).

Following *GAL-I-Sce1* induction, DSBs at *ade2-I* were repaired via gene conversion with *ade2-n* when both sister chromatids were cleaved in G2 cells. The pattern of gene conversion tracts was determined by colony color: solid white for short tract gene conversion on both sisters, sectored for short tract on one and long tract on the other, and solid red for long tract on both sisters (Supplementary Fig. S6A). We found a similar ratio of long tract versus short tract gene conversion (Supplementary Fig. S6B) and observed no chromosome loss events in any of the mutants tested (Supplementary Table S1).

The repair outcomes were determined by the sensitivity of cells to the antibiotic drugs Nat and hygromycin B (Hph) (Fig. 6B). Repair to NCO events results in Hph and Nat resistance (H^RN^R/H^RN^R), while repair to CO events leads to either Hph or Nat sensitivity (H^RN^S/H^SN^R). Repair by BIR events result in Nat resistance (H^SN^R/H^RN^R) (Fig. 6B). The most definitive determinant of repair outcomes was observed through the analysis of sectored colonies. In WT cells, sectored colonies exhibited a nearly even distribution of CO to NCO events, along with a small percentage of BIR events, consistent with the original study (Fig. 6C) [67]. We observed a reduction in CO events in *bre1Δ* and *htbKR* mutants, accompanied by an increase in BIR events, but only in *bre1Δ* and *htbKR* mutants; no such increase was observed in *fun30Δ* and *fun30Δ htbKR* mutants (Fig. 6C). The reduced CO was also evident in *bre1Δ* and *htbKR* mutants when measuring solid red colonies (Fig. 6D) and solid white colonies (Supplementary Fig. S6C). Similarly, the increased BIR was also observed in *bre1Δ* and *htbKR* mutants when analyzing solid red colonies (Fig. 6D), whereas no such increase was noted in solid white colonies. Solid white colonies underwent two short tract conversion events, for which NCO is the preferred repair outcome. In these cells, only a limited amount of CO and BIR were observed even in WT (Supplementary Fig. S6C). Remarkably, the occurrence of BIR events in *fun30Δ htbKR* mutants closely resembled that of the WT cells across all types of colonies examined (sectored, red, and white) (Fig. 6C and D and Supplementary Fig. S6C). In sum, these data show that the influence of H2Bubi on D-loop metabolism can significantly affect HR sub-pathway usage and outcome.

To validate the observed repair outcome in the diploid system, we employed a well-established physical recombination assay in haploid cells [65]. Haploid strains featuring an HO cut site insertion within the native *URA3* locus (*ura3-HO*) on Chr. V, alongside a 5.6-kb *ura3-HOinc* (non-cleavable) fragment integrated at the *LYS2* locus on Chr. II (Fig. 6E). Upon *GAL-HO* induction, the DSB on Chr. V undergoes repair via gene conversion, transferring the *ura3-HOinc* allele from Chr. II to Chr. V. The physical analysis was conducted at 0, 2, and 8 h, longer timepoints are difficult to interpret as cells that repair the DSB resume growth. To assess DSB repair efficiency, we examined the plating efficiency (PE) of each strain on galactose-containing medium compared with glucose-containing medium. Our analysis revealed a significantly lower PE for the *htbKR* mutant compared with the WT (Fig. 6F), demonstrating an involvement of H2Bubi in DSB repair. To ascertain the repair outcome, we induced HO in liquid cultures and isolated DNA at various timepoints post-HO induction for restriction digestion and southern blot hybridization. Mutants displaying decreased viability may be associated with the use of the BIR pathway, leading to the loss of essential genes downstream of the *ura3-HO* site, thereby resulting in lower PE. Since BIR and CO events are indistinguishable in the physical assay, we corrected the CO signal determined by Southern blot hybridization to the PE of all examined strains (Fig. 6G), as done in previous studies [66, 99]. The analysis revealed a two-fold decrease in CO events in the *htbKR* mutant compared with the WT (Fig. 6G). Intriguingly, *fun30Δ* rescues both PE and CO in the *htbKR* mutant, highlighting the inverse relationship between H2Bubi and Fun30 in DSB repair (Fig. 6F and G).

Collectively, we conclude that the impact of H2Bubi on D-loop metabolism can influence the usage of HR sub-pathways. If not tightly regulated, BIR may be used for repair, a process demonstrated to be mutagenic [100].

Discussion

H2Bubi has previously been associated with DSB repair [53–56, 101], yet the precise molecular mechanisms underlying its involvement in D-loop metabolism and its impact on repair outcome have remained poorly understood. Primer extension and ChIP assays are well-established and widely used to monitor DLE and detect Rad51 recruitment in studies of HR during mating-type switching [102–104]. In this study, we use the novel and validated DLC and DLE assays to identify and measure critical recombination intermediates during BIR, namely nascent and extended D-loops [19, 37]. These assays offer a unique advantage with their ability to directly detect these intermediates, setting them apart from techniques that rely on measuring the recruitment of recombinase Rad51 and physical or genetic repair endpoints. Rad51 measurement methods can suffer from non-specific issues, as Rad51 presence can be triggered by various forms of DNA damage beyond HR, for

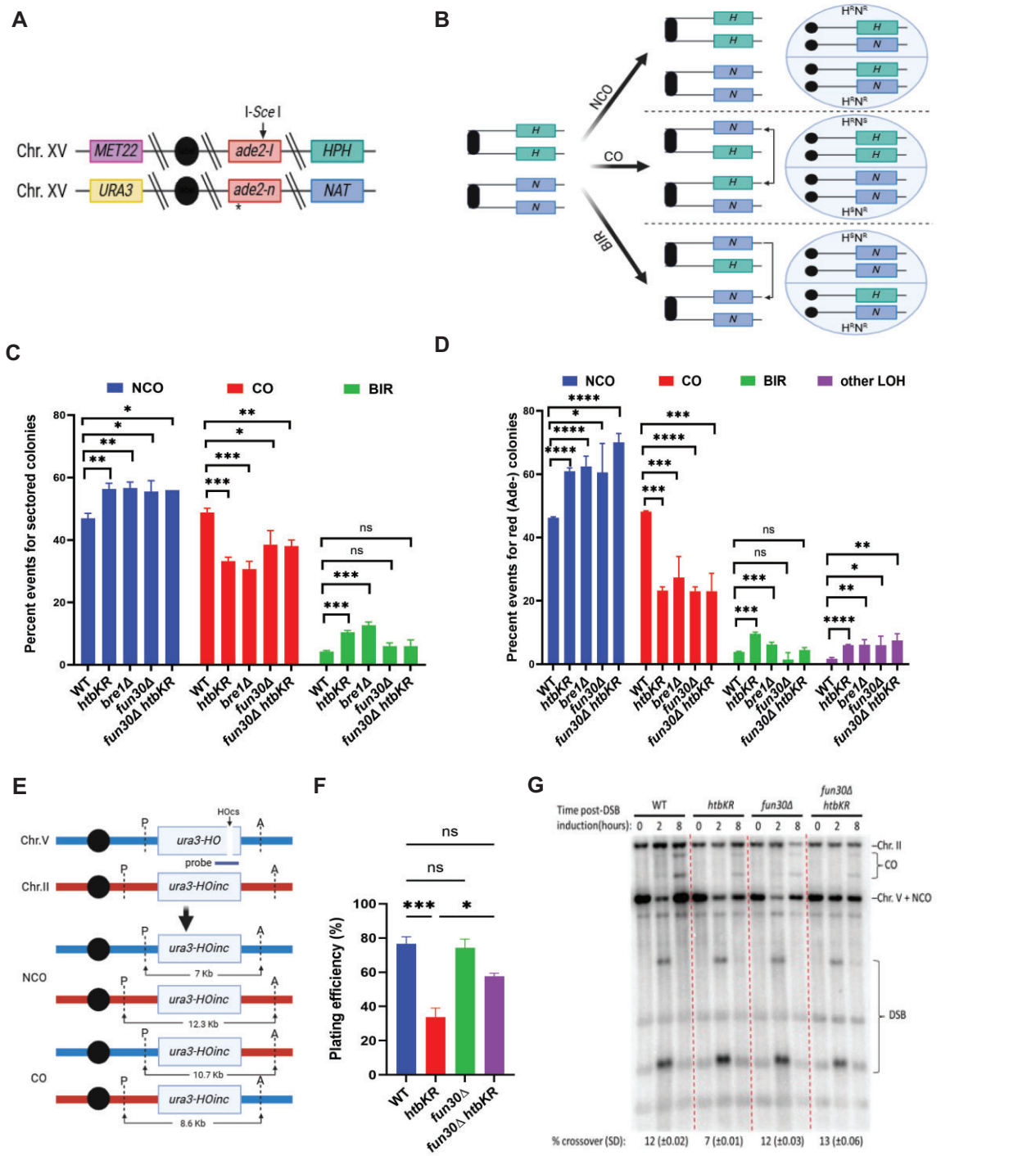

Figure 6. H2Bubi affects DSB repair pathway usage and outcome. (**A**) Schematic representation of the diploid strain, indicating the *I-SCE*1 cut site and the selection markers for determining repair outcomes and monitoring chromosome loss events (see text for details). (**B**) Schematic representation of repair outcomes, illustrating unchanged Nat and Hph markers in NCO repair, reciprocal exchange of Nat and Hph markers in CO repair, and non-reciprocal exchange of Nat and Hph markers in BIR, resulting in homozygosis of the Nat marker. H: Hph, N: Nat, R: resistance, S: sensitive. (**C**) Percentage of NCO, CO, and BIR events for sector colonies among the indicated strains. Error bars, SEM ($n \geq 2$). $^{***}P < .0007$, $^{**}P < .01$, $^{*}P < .04$, ns: not significant. (**D**) Percentage of occurrences for each strain within the red colonies. Error bars, SEM ($n \geq 2$). $^{****}P < .0001$, $^{***}P < .0008$, $^{**}P < .003$, $^{*}P < .03$, ns: not significant. (**E**) Schematic representation of the Chr. II–Chr. V ectopic recombination assay, depicting the distance between the HO endonuclease cut site (HO) and the heterology *Apa*LI (A) and *Pvu*II (P) sites located outside the region of shared homology were utilized to detect CO. Sizes of parental, NCO, and CO fragments are indicated. (**F**) PE was assessed by counting colony formation on YP-Gal plates divided by YP-Glu plates for each of the indicated strains across three independent trials. Error bars, SEM ($n = 3$). $^{*}P = .02$, $^{***}P < .0007$, ns: not significant. (**G**) Southern blot analysis was conducted on DNA extracted from cells sampled at 0, 2, and 8 h post-DSB induction. Genomic DNA from each strain was digested with *Pvu*II and *Apa*LI enzymes, then probed with a fragment of Chr. V carrying the *URA3* gene. The percentage of CO product at the 8-h timepoint was calculated using densitometer quantification. This percentage was obtained by dividing the intensity of CO bands by the total DNA content (Chr. II, Chr. V, and CO). Subsequently, the CO level was normalized to the plating efficiency obtained from panel (E). The numbers in parentheses represent the standard deviation values obtained from three independent trials. Fig. 6A, B, and E were created in BioRender.com.

example stalled forks for fork protection [105]. Furthermore, the DLC and DLE assays diverge from genetic analysis, which primarily focuses on providing insights into repair outcomes but lacks the necessary detail to fully understand molecular mechanism of the recombination process.

By using DLC and DLE assays to monitor D-loop metabolism, alongside physical and genetic assays to detect repair outcomes in cells lacking H2Bubi and various mutants affecting chromatin, we have uncovered multifaceted functions of H2Bubi in D-loop metabolism. H2Bubi finely regulates chromatin structure: first, it facilitates histone degradation as shown by the Gasser laboratory [56], thus promoting the formation of nascent D-loops. Second, it potentially stabilizes extended D-loops likely through nucleosome assembly. Third, H2Bubi regulates DNA resection—it coordinates the kinetics of DNA resection with the kinetics of D-loop formation and DLE by recruiting Rad9 (Fig. 7).

H2Bubi facilitates nascent D-loop formation

Our study offers evidence demonstrating the impact of H2Bubi on nascent D-loop formation and DLE. Notably, the deficiency in nascent D-loop formation can be restored by eliminating factors involved in the D-loop disruption pathways identified in our previous research [19], underscoring the critical role of the D-loop disruption pathway in monitoring nascent D-loops. Furthermore, manipulating chromatin structure by removing factors known to alter chromatin structure through various mechanisms influences nascent D-loop levels to varying degrees. Our studies provide several line of evidences to suggest that H2bubi fine-tunes chromatin structure for HR: first, we demonstrated that *ARP8* deletion, previously associated with compacted chromatin, resulted in a dramatic reduction in nascent D-loop formation, similar to the *htbKR* mutant, which is congruent with previous studies suggesting that Rad6 and Bre1 recruitment upon DNA damage depends on INO80 [56]. Conversely, the *NHP6A/B* deletion, previously linked to expanded chromatin, showed complete rescue of the D-loop defect in *htbKR*, likely due to a 20% reduction in histone occupancy [56, 77, 79]. Moreover, our epistasis analysis revealed that Hho1 acts downstream of H2Bubi, consistent with previous studies proposing core and linker histone degradation upon DNA damage [56, 76]. Our study further defines H2Bubi's role as upstream of linker histone Hho1. Second, our epistasis analysis shows that the histone chaperones Asf1 and CAF-1 act upstream of H2Bubi, consistent with their role in promoting the assembly and disassembly of nucleosomes. Our results demonstrate that reducing histone occupancy by deleting *ASF1* or *CAC1* reverses the decompaction defect observed in the *htbKR* mutant. Third, our epistasis analysis reveals that the histone variant H2A.Z acts upstream of H2Bubi, which is intriguing. One possible explanation is that in the absence of H2Bubi, H2A.Z inhibits Rad51 filament formation, similar to previous reports showing restoration of presynaptic filament formation and HR in INO80-C-deficient mutants when H2A.Z is absent [86]. It is worth noting that the restored nascent D-loop level in the *htz1Δ htbKR* double mutant can be explained by the restored presynaptic filament formation. Furthermore, we observed that the deposition of H2A.Z also play a role in promoting nascent D-loop formation, as evidenced by the reduced DLC levels in *swr1Δ* and *htz1Δ* mutants. Our results reveal a complex role for H2A.Z in nascent D-loop formation, consistent with previous studies demonstrating that H2A.Z is deposited to promote DNA resection and later removed during Rad51 filament formation [84–86]. In conclusion, we infer that INO80 acts upstream of H2Bubi through H2A.Z removal to promote proteasome-dependent histone degradation [56], which promotes Rad51 filament formation as a prerequisite for homology search and nascent D-loop formation (Fig. 7).

H2Bubi promotes nascent D-loop formation by facilitating histone degradation and stabilizes extended D-loop via nucleosome assembly

H2Bubi stands out as one of the most significant chromatin marks known in the regulation of chromatin structure and compaction [52]. However, the mechanism by which H2Bubi fine-tunes chromatin structure to facilitate HR during D-loop metabolism remains unclear. Our study provides evidence demonstrating that H2Bubi promotes nascent D-loop formation through histone degradation [56] (Fig. 3), while stabilizing the extended D-loop via chromatin assembly (Fig. 4). This hypothesis is supported by several lines of evidence: first, removing D-loop disruption pathways significantly recovered nascent D-loop levels in the *htbKR* mutant, while extended D-loop levels remained low (Supplementary Fig. S7A and D-loop disruption category). Second, the reduction of histone occupancy restored nascent D-loop levels but did not rescue extended D-loop levels in the *htbKR* mutant. This suggests that H2Bubi stabilizes the extended D-loop through chromatin assembly, rather than promoting chromatin disassembly ahead of it (Supplementary Fig. S7A, chromatin structure category). Indeed, we observed that H2Bubi levels are enriched at the DLE regions, but not at other regions of the donor site (Fig. 4J). This may resemble DNA replication, where H2Bubi promotes chromatin assembly behind the replication fork [106, 107]. Similarly, we speculate that H2Bubi may stabilize the extended D-loop by chromatin assembly at or behind the D-loop (Fig. 7). This may involve not only full nucleosomes but possibly also histoner dimers or tetramers and potentially noncanonicaly ways of engaging with DNA as speculated in Fig. 7B. In sum, the results suggest that the DLE defect in the *htbKR* mutant is not the simple downstream consequence of the defect in D-loop levels and not solely caused by a defect in Rad51–ssDNA filament assembly. Rather, we interpret that these phenotypes reflect the complex roles of chromatin on different steps of the HR process.

Moreover, the direct interaction between Bre1 with RPA, Rad51, and Srs2 [87, 108] raises the possibility that Bre1 may be recruited to extended D-loops through RPA, Rad51, and Srs2 binding, enhancing local H2Bubi levels to facilitate DNA synthesis during DLE. However, this needs further investigation.

Our study observed no significant effect of Asf1 and CAF-1 on DLE during the repair of a two-sided (frank) DSB. In a different functional context, recombination-dependent replication in fission yeast, both were founds required for DNA synthesis [49, 50], which may reflect the difference between HR during template switching at stalled forks where HR intermediates may be stabilized by histone deposition.

Additionally, it has been shown that the human homolog of Fun30, SMARCAD1, directly interacts with the PCNA replication clamp and is preferentially enriched at unperturbed replication forks, suggesting a role in DNA replication [109]. Our study reveals a novel function of Fun30 that inversely cor-

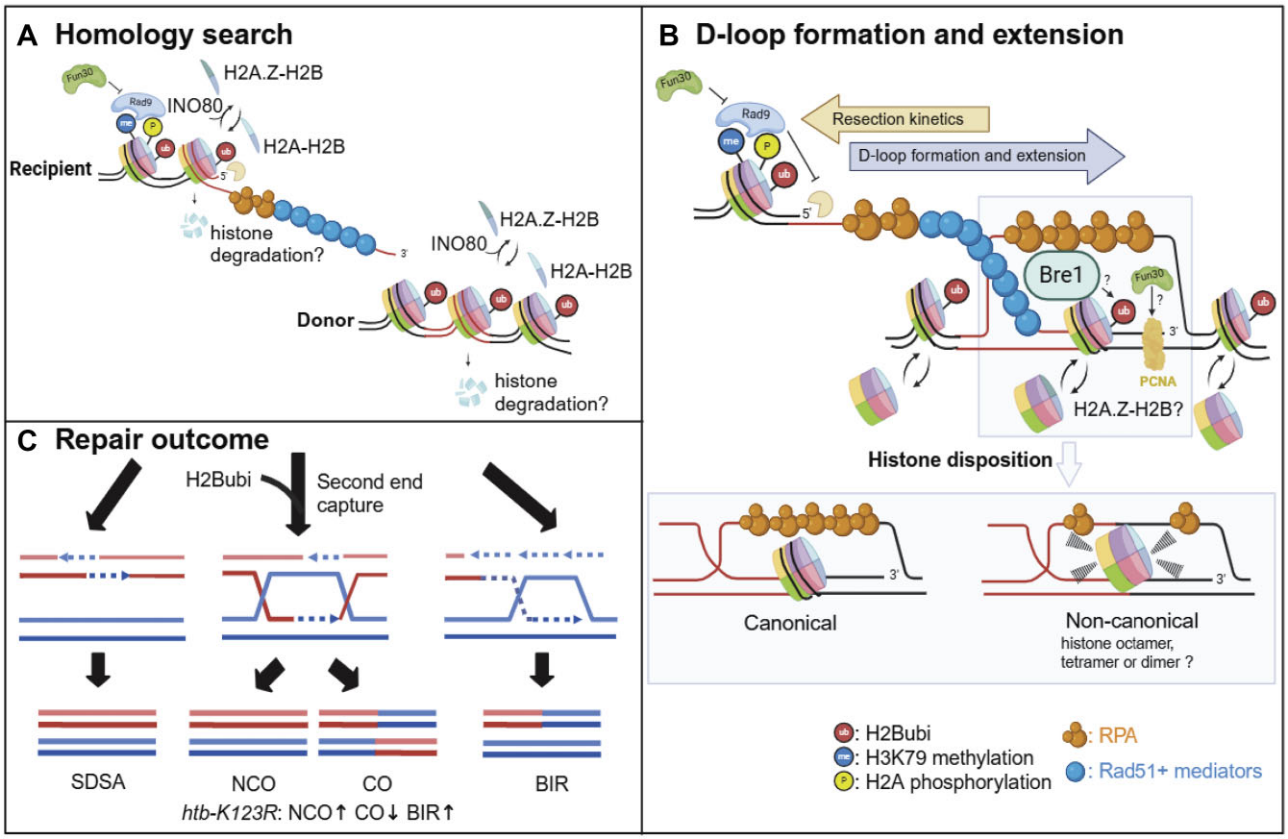

Figure 7. Model depicting the regulation of D-loop metabolism and repair outcomes by H2Bubi H2Bubi may regulate D-loop metabolism through several mechanisms: (**A**) by promoting histone degradation, as shown in [56], to facilitate homology search and nascent D-loop formation; (**B**) by coordinating DNA resection with D-loop formation and DLE through Rad9 recruitment and stabilizing the extended D-loop via nucleosome assembly. The epistatic relationship between H2Bubi, Fun30, and H2A.Z suggests potential cooperation in DNA resection and D-loop metabolism; (**C**) H2Bubi may also influence second-end capture, potentially shifting repair from CO to BIR. Fig. 7 was created in BioRender.com.

relates with H2Bubi in DLE. Whether this correlation relates to its replication function requires further investigation.

Recent cryo-electron microscopic structural studies have revealed that H2A.Z destabilizes the nucleosome structure by enhancing DNA mobility near the DNA entry/exit site, while also facilitating the formation of more regular and compact chromatin fiber in nucleosome arrays [110]. The interplay between H2Bubi and H2A.Z contributes to transcriptional regulation in a context-dependent manner [111, 112]. This suggests that H2Bubi may influence nascent D-loop formation and DLE by stabilizing H2A.Z in nucleosomes or hindering its eviction, and *vice versa*.

Due to the structural similarity between the Fun30 with the INO80 and SWR complexes, Fun30 may play a role in histone dimer exchange [113, 114]. It has been shown that *FUN30* genetically interacts with subunits of the SWR complex and histone H2A.Z [115] and *FUN30* deletion results in defects in genome-wide histone variant H2A.Z occupancy, further supporting this notion [116]. Our study reveals that the cross talk between H2Bubi, H2A.Z, INO80, SWR1, and Fun30 provides a possibility that their interaction may fine-tune chromatin structure for D-loop metabolism (Fig. 7).

Resection influences D-loop metabolism

The rate of resection, necessary to produce ssDNA for homology search, may serve as a time-limiting factor for the homology search process. Initially, the formed 3′ ssDNA is coated by RPA, followed by Rad51 filament formation, which facilitates the search for a homologous sequence. If successful, this search is succeeded by the invasion of the template sequence. Surprisingly, hyper-resection in cells lacking H2Bubi does not result in successful strand invasion, indicating that excessive resection negatively affects D-loop levels (Fig. 5). Consistently, we observed that slowing down resection kinetics by deleting *FUN30* restored the kinetics of nascent D-loop formation and DLE in the *htbKR* mutant (Fig. 5D and G). Furthermore, we found that the reduced cell viability, decreased CO formation and increased BIR observed in the *htbKR* mutant were restored to WT levels in the *fun30Δ htbKR* double mutant (Fig. 6C, D, F, and G).

This suggests that H2Bubi may play an additional role in sustaining the kinetics of D-loop formation and DLE by limiting excessive DNA end resection through recruiting Rad9 (Supplementary Fig. S7A, chromatin factors affecting Rad9 recruitment). This finding is supported by research suggesting that Rad9 has an additional function independent of Rad53 checkpoint signaling in stabilizing D-loops by limiting the recruitment of proteins involved in D-loop disruption pathways [117]. Additionally, this research suggests that in the absence of Rad9, hyperactivating of Mec1 signaling regulates the STR-dependent D-loop disruption pathway to influence HR outcomes and suppress gross chromosomal rearrangements [118, 119]. Moreover, Rad9's function in Rad53 checkpoint signal-

ing has been demonstrated to prevent aberrant processing of BIR intermediates [120]. In sum, these results suggest the existence of a negative feedback loop between resection and D-loop reversal that safeguards the homology search process to limit non-allelic HR and gross chromosomal rearrangements (Fig. 7B). Alternatively, prolonged checkpoint activation in *fun30Δ* cells may promote D-loop formation and DLE through an unknown mechanism.

The dependence of H3K79 methylation on H2Bubi is an example of histone modification cross talk that is conserved across eukaryotes [121, 122]. One of the functions of H3K79 methylation is to regulate the DNA damage checkpoint response and DNA resection through Rad9 chromatin recruitment, which acts as a Mec1 adaptor for Rad53 activation and also serves as a barrier to inhibit DNA resection [60, 89, 123]. In contrast, Fun30, a chromatin remodeler, promotes DNA resection by antagonizing Rad9. Despite multiple studies, the mechanism by which Fun30 removes Rad9 remains unknown [124]. Fun30 possesses a CUE domain, which is known for its ability to bind ubiquitin [125]. Whether Fun30 binds H2Bubi through its CUE domain remains an open question and warrants further investigation. One possible scenario is that H2Bubi itself recruits Fun30 to promote DNA resection and checkpoint deactivation. On the other hand, downstream H3K79 methylation may mediate Rad9 chromatin recruitment, thereby inhibiting DNA resection and checkpoint activation. Together, these processes could fine-tune DNA resection and the DNA damage checkpoint response.

H2Bubi affects DSB repair pathway usage and outcome

D-loops serve as a central intermediate of HR-mediated repair. Therefore, if any issue arises during D-loop metabolism, the frequencies BIR, CO, and NCO may be affected. To this end, we examined the competition between DSB repair sub-pathways using genetic and physical assays (Fig. 6). In the DLC/E and BIR assays, DSBs are exclusively repaired by the BIR pathway (Fig. 1) not allowing to study competition between HR sub-pathways. In competition assays, we consistently observed an increase in BIR and a decrease in CO outcomes by analysis of genetic and physical endpoints in cells lacking H2Bubi. BIR events could arise due to the failure of second end capture thus discourage the formation of double Holliday junctions and subsequent COs [4, 5].

Our results provide evidence to explain why CO decreases and BIR increases in the absence of H2Bubi. The kinetics of nascent and extended D-loops are dramatically delayed in cells lacking H2Bubi, consistent with the hypothesis that limiting the lifetime of nascent and extended D-loops discourages the formation of dHJs and subsequent COs. Moreover, our observation is supported by a previous study demonstrating reduced meiotic COs upon depletion of the E3 ligase RNF20 for H2Bubi in mice [57]. Finally, inappropriate DNA resection may interfere with engaging the second end either by annealing and strand invasion. It is also possible that H2Bubi may influence the competition between gene conversion and BIR through Sgs1 and Mph1, as it has been reported that these proteins play major roles in shifting between gene conversion and BIR [126]. This potential mechanism cannot be excluded by this study and warrants further investigation.

We conclude that the effect of H2Bubi on D-loop metabolism can influence repair pathway usage (Fig. 7C). Specifically, H2Bubi plays a crucial role in preventing BIR, a sub-pathway of DNA DSB repair known to culminate in genomic instability.

Limitations of the study

In this study, we reveal that H2Bubi plays multifaceted roles in regulating the kinetics of nascent D-loop formation and DLE. However, due to the technical constraints of visualizing nucleosomes on extended D-loops, we still do not fully understand how H2Bubi stabilizes extended D-loops. Additionally, the molecular mechanism by which H2Bubi coordinates DNA resection and D-loop formation is lacking. Further studies analyzing resection intermediates would provide a clearer interpretation of this molecular mechanism. H2Bubi controls H3 methylation through Dot1-mediated H3K79 and Set1-mediated H3K4 methylation [59]. While previous studies suggest that the HR repair function of H2Bubi is independent of H3K4 or H3K79 methylation [55], we cannot definitively state whether the effect we observe are directly or indirectly caused by H2Bubi.

In addition, this study uses several chromatin mutants in DLC/E assays to investigate how these mutants affect D-loop formation and DLE, without directly measuring chromatin structure alterations. These chromatin mutants, such as *nhp6ΔΔ*, have been previously reported to influence nucleosome occupancy based on MNase sequencing [79]. Further characterization using newer methodologies, such as fiber sequencing, may be required to provide insights into nucleosome organization at the single-fiber level [127]. Moreover, the genome-wide localization of H2Bubi needs to be carefully examined to compare its level at DSBs, the donor site, and other regions of the genome.

Furthermore, due to the technical constraints of detecting D-loop size *in vivo* and the fact that nucleosomes are not well-positioned at the homology donor, we are unable to determine the average size of D-loops in WT cells compared with mutants, nor can we assess how many nucleosomes are physically assembled on the dsDNA portion of the D-loop during extension.

Acknowledgements

We express our gratitude to the members of the Heyer laboratory, especially Diedre Reitz, for their valuable discussions. We thank Susan Gasser and Marcus Smolka for insightful comments on the manuscript. We also extend our thanks to Lorraine Symington, Marcus Smolka, and Cheng-Fu Kao for providing yeast strains and plasmids. The graphical abstract was created with BioRender.com.

Author contributions: S.-H.H. and W.-D.H. conceived the project and drafted the manuscript. S.-H.H. designed, conducted, and analyzed the experiments. Y.L. contributed to the experimental work and analysis.

Supplementary data

Supplementary data is available at NAR online.

Conflict of interest

None declared.

Funding

This work received support from NIH awards R01GM58015 and R01GM137751 granted to W.-D.H. and the Cancer Center Core Support grant P30CA093373. Additionally, S.-H.H acknowledges partial support from a fellowship provided by Academia Sinica, Taiwan. Funding to pay the Open Access publication charges for this article was provided by NIH.

Data availability

The data underlying this article are available in the article and in its online supplementary material.

References

1. Symington LS. End resection at double-strand breaks: mechanism and regulation. *Cold Spring Harb Perspect Biol* 2014;**6**:a016436. https://doi.org/10.1101/cshperspect.a016436
2. Cejka P, Symington LS. DNA end resection: mechanism and control. *Annu Rev Genet* 2021;**55**:285–307. https://doi.org/10.1146/annurev-genet-071719-020312
3. Heyer WD, Ehmsen KT, Liu J. Regulation of homologous recombination in eukaryotes. *Annu Rev Genet* 2010;**44**:113–39. https://doi.org/10.1146/annurev-genet-051710-150955
4. Wright WD, Shah SS, Heyer WD. Homologous recombination and the repair of DNA double-strand breaks. *J Biol Chem* 2018;**293**:10524–35. https://doi.org/10.1074/jbc.TM118.000372
5. Piazza A, Heyer WD. Moving forward one step back at a time: reversibility during homologous recombination. *Curr Genet* 2019;**65**:1333–40. https://doi.org/10.1007/s00294-019-00995-7
6. Heyer WD. Regulation of recombination and genomic maintenance. *Cold Spring Harb Perspect Biol* 2015;**7**:a016501. https://doi.org/10.1101/cshperspect.a016501
7. Liu J, Renault L, Veaute X *et al.* Rad51 paralogues Rad55–Rad57 balance the antirecombinase Srs2 in Rad51 filament formation. *Nature* 2011;**479**:245–8. https://doi.org/10.1038/nature10522
8. Krejci L, Van Komen S, Li Y *et al.* DNA helicase Srs2 disrupts the Rad51 presynaptic filament. *Nature* 2003;**423**:305–9. https://doi.org/10.1038/nature01577
9. Antony E, Tomko EJ, Xiao Q *et al.* Srs2 disassembles Rad51 filaments by a protein-protein interaction triggering ATP turnover and dissociation of Rad51 from DNA. *Mol Cell* 2009;**35**:105–15. https://doi.org/10.1016/j.molcel.2009.05.026
10. Burgess RC, Lisby M, Altmannova V *et al.* Localization of recombination proteins and Srs2 reveals anti-recombinase function *in vivo*. *J Cell Biol* 2009;**185**:969–81. https://doi.org/10.1083/jcb.200810055
11. Dupaigne P, Le Breton C, Fabre F *et al.* The Srs2 helicase activity is stimulated by Rad51 filaments on dsDNA: implications for crossover incidence during mitotic recombination. *Mol Cell* 2008;**29**:243–54. https://doi.org/10.1016/j.molcel.2007.11.033
12. Van Komen S, Reddy MS, Krejci L *et al.* ATPase and DNA helicase activities of the *Saccharomyces cerevisiae* anti-recombinase Srs2. *J Biol Chem* 2003;**278**:44331–7. https://doi.org/10.1074/jbc.M307256200
13. Krejci L, Macris M, Li Y *et al.* Role of ATP hydrolysis in the antirecombinase function of *Saccharomyces cerevisiae* Srs2 protein. *J Biol Chem* 2004;**279**:23193–9. https://doi.org/10.1074/jbc.M402586200
14. Ma E, Dupaigne P, Maloisel L *et al.* Rad52–Rad51 association is essential to protect Rad51 filaments against Srs2, but facultative for filament formation. *eLife* 2018;**7**:e32744. https://doi.org/10.7554/eLife.32744
15. Roy U, Kwon Y, Marie L *et al.* The Rad51 paralog complex Rad55–Rad57 acts as a molecular chaperone during homologous recombination. *Mol Cell* 2021;**81**:1043–57. https://doi.org/10.1016/j.molcel.2020.12.019
16. Veaute X, Jeusset J, Soustelle C *et al.* The Srs2 helicase prevents recombination by disrupting Rad51 nucleoprotein filaments. *Nature* 2003;**423**:309–12. https://doi.org/10.1038/nature01585
17. Cejka P, Plank JL, Dombrowski CC *et al.* Decatenation of DNA by the *S. cerevisiae* Sgs1–Top3–Rmi1 and RPA complex: a mechanism for disentangling chromosomes. *Mol Cell* 2012;**47**:886–96. https://doi.org/10.1016/j.molcel.2012.06.032
18. Fasching CL, Cejka P, Kowalczykowski SC *et al.* Top3–Rmi1 dissolve Rad51-mediated D loops by a topoisomerase-based mechanism. *Mol Cell* 2015;**57**:595–606. https://doi.org/10.1016/j.molcel.2015.01.022
19. Piazza A, Shah SS, Wright WD *et al.* Dynamic processing of displacement loops during recombinational DNA repair. *Mol Cell* 2019;**73**:1255–66. https://doi.org/10.1016/j.molcel.2019.01.005
20. Lo YC, Paffett KS, Amit O *et al.* Sgs1 regulates gene conversion tract lengths and crossovers independently of its helicase activity. *Mol Cell Biol* 2006;**26**:4086–94. https://doi.org/10.1128/MCB.00136-06
21. Wu L, Hickson ID. The Bloom's syndrome helicase suppresses crossing over during homologous recombination. *Nature* 2003;**426**:870–4. https://doi.org/10.1038/nature02253
22. Liu J, Ede C, Wright WD *et al.* Srs2 promotes synthesis-dependent strand annealing by disrupting DNA polymerase delta-extending D-loops. *eLife* 2017;**6**:e22195. https://doi.org/10.7554/eLife.22195
23. Mitchel K, Lehner K, Jinks-Robertson S. Heteroduplex DNA position defines the roles of the Sgs1, Srs2, and Mph1 helicases in promoting distinct recombination outcomes. *PLoS Genet* 2013;**9**:e1003340. https://doi.org/10.1371/journal.pgen.1003340
24. Prakash R, Satory D, Dray E *et al.* Yeast Mph1 helicase dissociates Rad51-made D-loops: implications for crossover control in mitotic recombination. *Genes Dev* 2009;**23**:67–79. https://doi.org/10.1101/gad.1737809
25. Polo SE, Almouzni G. Chromatin dynamics after DNA damage: the legacy of the access-repair-restore model. *DNA Repair (Amst)* 2015;**36**:114–21. https://doi.org/10.1016/j.dnarep.2015.09.014
26. Chakraborty U, Shen ZJ, Tyler J. Chaperoning histones at the DNA repair dance. *DNA Repair (Amst)* 2021;**108**:103240. https://doi.org/10.1016/j.dnarep.2021.103240
27. Mohan C, Das C, Tyler J. Histone and chromatin dynamics facilitating DNA repair. *DNA Repair (Amst)* 2021;**107**:103183. https://doi.org/10.1016/j.dnarep.2021.103183
28. Peterson CL, Almouzni G. Nucleosome dynamics as modular systems that integrate DNA damage and repair. *Cold Spring Harb Perspect Biol* 2013;**5**:a012658. https://doi.org/10.1101/cshperspect.a012658
29. Papamichos-Chronakis M, Peterson CL. Chromatin and the genome integrity network. *Nat Rev Genet* 2013;**14**:62–75. https://doi.org/10.1038/nrg3345
30. Hauer MH, Gasser SM. Chromatin and nucleosome dynamics in DNA damage and repair. *Genes Dev* 2017;**31**:2204–21. https://doi.org/10.1101/gad.307702.117
31. Seeber A, Hauer MH, Gasser SM. Chromosome dynamics in response to DNA damage. *Annu Rev Genet* 2018;**52**:295–319. https://doi.org/10.1146/annurev-genet-120417-031334
32. Smeenk G, van Attikum H. The chromatin response to DNA breaks: leaving a mark on genome integrity. *Annu Rev Biochem* 2013;**82**:55–80. https://doi.org/10.1146/annurev-biochem-061809-174504
33. Seeber A, Hauer M, Gasser SM. Nucleosome remodelers in double-strand break repair. *Curr Opin Genet Dev* 2013;**23**:174–84. https://doi.org/10.1016/j.gde.2012.12.008
34. van Attikum H, Gasser SM. Crosstalk between histone modifications during the DNA damage response. *Trends Cell Biol* 2009;**19**:207–17. https://doi.org/10.1016/j.tcb.2009.03.001
35. Price BD, D'Andrea AD. Chromatin remodeling at DNA double-strand breaks. *Cell* 2013;**152**:1344–54. https://doi.org/10.1016/j.cell.2013.02.011

36. Garcia Fernandez F, Fabre E. The dynamic behavior of chromatin in response to DNA double-strand breaks. *Genes* 2022;**13**:215. https://doi.org/10.3390/genes13020215
37. Piazza A, Koszul R, Heyer WD. A proximity ligation-based method for quantitative measurement of D-loop extension in *S. cerevisiae*. *Methods Enzymol* 2018;**601**:27–44. https://doi.org/10.1016/bs.mie.2017.11.024
38. Donnianni RA, Symington LS. Break-induced replication occurs by conservative DNA synthesis. *Proc Natl Acad Sci USA* 2013;**110**:13475–80. https://doi.org/10.1073/pnas.1309800110
39. Jain S, Sugawara N, Lydeard J *et al.* A recombination execution checkpoint regulates the choice of homologous recombination pathway during DNA double-strand break repair. *Genes Dev* 2009;**23**:291–303. https://doi.org/10.1101/gad.1751209
40. Groth A, Corpet A, Cook AJ *et al.* Regulation of replication fork progression through histone supply and demand. *Science* 2007;**318**:1928–31. https://doi.org/10.1126/science.1148992
41. Lydeard JR, Jain S, Yamaguchi M *et al.* Break-induced replication and telomerase-independent telomere maintenance require Pol32. *Nature* 2007;**448**:820–3. https://doi.org/10.1038/nature06047
42. Liu L, Yan Z, Osia BA *et al.* Tracking break-induced replication shows that it stalls at roadblocks. *Nature* 2021;**590**:655–9. https://doi.org/10.1038/s41586-020-03172-w
43. McVey M, Khodaverdian VY, Meyer D *et al.* Eukaryotic DNA polymerases in homologous recombination. *Annu Rev Genet* 2016;**50**:393–421. https://doi.org/10.1146/annurev-genet-120215-035243
44. Li X, Stith CM, Burgers PM *et al.* PCNA is required for initiating recombination-associated DNA synthesis by DNA polymerase δ. *Mol Cell* 2009;**36**:704–13. https://doi.org/10.1016/j.molcel.2009.09.036
45. Sneeden JL, Grossi SM, Tappin I *et al.* Reconstitution of recombination-associated DNA synthesis with human proteins. *Nucleic Acids Res* 2013;**41**:4913–25. https://doi.org/10.1093/nar/gkt192
46. Reitz D, Djeghmoum Y, Watson RA *et al.* Delineation of two multi-invasion-induced rearrangement pathways that differently affect genome stability. *Genes Dev* 2023;**37**:621–39. https://doi.org/10.1101/gad.350618.123
47. Ransom M, Dennehey BK, Tyler JK. Chaperoning histones during DNA replication and repair. *Cell* 2010;**140**:183–95. https://doi.org/10.1016/j.cell.2010.01.004
48. Groth A, Rocha W, Verreault A *et al.* Chromatin challenges during DNA replication and repair. *Cell* 2007;**128**:721–33. https://doi.org/10.1016/j.cell.2007.01.030
49. Hardy J, Dai D, Ait Saada A *et al.* Histone deposition promotes recombination-dependent replication at arrested forks. *PLoS Genet* 2019;**15**:e1008441. https://doi.org/10.1371/journal.pgen.1008441
50. Pietrobon V, Freon K, Hardy J *et al.* The chromatin assembly factor 1 promotes Rad51-dependent template switches at replication forks by counteracting D-loop disassembly by the RecQ-type helicase Rqh1. *PLoS Biol* 2014;**12**:e1001968. https://doi.org/10.1371/journal.pbio.1001968
51. Juhasz S, Elbakry A, Mathes A *et al.* ATRX promotes DNA repair synthesis and sister chromatid exchange during homologous recombination. *Mol Cell* 2018;**71**:11–24. https://doi.org/10.1016/j.molcel.2018.05.014
52. Fierz B, Chatterjee C, McGinty RK *et al.* Histone H2B ubiquitylation disrupts local and higher-order chromatin compaction. *Nat Chem Biol* 2011;**7**:113–9. https://doi.org/10.1038/nchembio.501
53. Moyal L, Lerenthal Y, Gana-Weisz M *et al.* Requirement of ATM-dependent monoubiquitylation of histone H2B for timely repair of DNA double-strand breaks. *Mol Cell* 2011;**41**:529–42. https://doi.org/10.1016/j.molcel.2011.02.015
54. Nakamura K, Kato A, Kobayashi J *et al.* Regulation of homologous recombination by RNF20-dependent H2B ubiquitination. *Mol Cell* 2011;**41**:515–28. https://doi.org/10.1016/j.molcel.2011.02.002
55. Zheng S, Li D, Lu Z *et al.* Bre1-dependent H2B ubiquitination promotes homologous recombination by stimulating histone eviction at DNA breaks. *Nucleic Acids Res* 2018;**46**:11326–39. https://doi.org/10.1093/nar/gky918
56. Challa K, Schmid CD, Kitagawa S *et al.* Damage-induced chromatome dynamics link ubiquitin ligase and proteasome recruitment to histone loss and efficient DNA repair. *Mol Cell* 2021;**81**:811–29. https://doi.org/10.1016/j.molcel.2020.12.021
57. Xu Z, Song Z, Li G *et al.* H2B ubiquitination regulates meiotic recombination by promoting chromatin relaxation. *Nucleic Acids Res* 2016;**44**:9681–97.
58. Yamashita K, Shinohara M, Shinohara A. Rad6–Bre1-mediated histone H2B ubiquitylation modulates the formation of double-strand breaks during meiosis. *Proc Natl Acad Sci USA* 2004;**101**:11380–5. https://doi.org/10.1073/pnas.0400078101
59. Game JC, Chernikova SB. The role of RAD6 in recombinational repair, checkpoints and meiosis via histone modification. *DNA Repair (Amst)* 2009;**8**:470–82. https://doi.org/10.1016/j.dnarep.2009.01.007
60. Giannattasio M, Lazzaro F, Plevani P *et al.* The DNA damage checkpoint response requires histone H2B ubiquitination by Rad6–Bre1 and H3 methylation by Dot1. *J Biol Chem* 2005;**280**:9879–86. https://doi.org/10.1074/jbc.M414453200
61. Tyler JK, Adams CR, Chen SR *et al.* The RCAF complex mediates chromatin assembly during DNA replication and repair. *Nature* 1999;**402**:555–60. https://doi.org/10.1038/990147
62. Guldener U, Heck S, Fielder T *et al.* A new efficient gene disruption cassette for repeated use in budding yeast. *Nucleic Acids Res* 1996;**24**:2519–24. https://doi.org/10.1093/nar/24.13.2519
63. Reitz D, Savocco J, Piazza A *et al.* Detection of homologous recombination intermediates via proximity ligation and quantitative PCR in *Saccharomyces cerevisiae*. *J Vis Exp* 2022;**187**:10.3791/64240. https://doi.org/10.3791/64240
64. Zierhut C, Diffley JF. Break dosage, cell cycle stage and DNA replication influence DNA double strand break response. *EMBO J* 2008;**27**:1875–85. https://doi.org/10.1038/emboj.2008.111
65. Aylon Y, Liefshitz B, Bitan-Banin G *et al.* Molecular dissection of mitotic recombination in the yeast *Saccharomyces cerevisiae*. *Mol Cell Biol* 2003;**23**:1403–17. https://doi.org/10.1128/MCB.23.4.1403-1417.2003
66. Mazon G, Symington LS. Mph1 and Mus81-Mms4 prevent aberrant processing of mitotic recombination intermediates. *Mol Cell* 2013;**52**:63–74. https://doi.org/10.1016/j.molcel.2013.09.007
67. Ho CK, Mazon G, Lam AF *et al.* Mus81 and Yen1 promote reciprocal exchange during mitotic recombination to maintain genome integrity in budding yeast. *Mol Cell* 2010;**40**:988–1000. https://doi.org/10.1016/j.molcel.2010.11.016
68. Bustin SA, Benes V, Garson JA *et al.* The MIQE guidelines: minimum information for publication of quantitative real-time PCR experiments. *Clin Chem* 2009;**55**:611–22. https://doi.org/10.1373/clinchem.2008.112797
69. Donnianni RA, Zhou ZX, Lujan SA *et al.* DNA polymerase delta synthesizes both strands during break-induced replication. *Mol Cell* 2019;**76**:371–81. https://doi.org/10.1016/j.molcel.2019.07.033
70. Fabre F, Chan A, Heyer WD *et al.* Alternate pathways involving Sgs1/Top3, Mus81/Mms4, and Srs2 prevent formation of toxic recombination intermediates from single-stranded gaps created by DNA replication. *Proc Natl Acad Sci USA* 2002;**99**:16887–92. https://doi.org/10.1073/pnas.252652399
71. Liu J, Renault L, Veaute X *et al.* Rad51 paralogs Rad55–Rad57 balance the anti-recombinase function of Srs2 in Rad51 pre-synaptic filament formation. *Nature* 2011;**479**:245–48. https://doi.org/10.1038/nature10522

72. Cejka P, Symington LS. DNA end resection: mechanism and control. *Annu Rev Genet* 2021;**55**:285–307. https://doi.org/10.1146/annurev-genet-071719-020312
73. Mimitou EP, Symington LS. Sae2, Exo1 and Sgs1 collaborate in DNA double-strand break processing. *Nature* 2008;**455**:770–4. https://doi.org/10.1038/nature07312
74. Gravel S, Chapman JR, Magill C *et al.* DNA helicases Sgs1 and BLM promote DNA double-strand break resection. *Genes Dev* 2008;**22**:2767–72. https://doi.org/10.1101/gad.503108
75. Zhu Z, Chung WH, Shim EY *et al.* Sgs1 helicase and two nucleases Dna2 and Exo1 resect DNA double-strand break ends. *Cell* 2008;**134**:981–94. https://doi.org/10.1016/j.cell.2008.08.037
76. Hauer MH, Seeber A, Singh V *et al.* Histone degradation in response to DNA damage enhances chromatin dynamics and recombination rates. *Nat Struct Mol Biol* 2017;**24**:99–107. https://doi.org/10.1038/nsmb.3347
77. Cheblal A, Challa K, Seeber A *et al.* DNA damage-induced nucleosome depletion enhances homology search independently of local break movement. *Mol Cell* 2020;**80**:311–26. https://doi.org/10.1016/j.molcel.2020.09.002
78. Seeber A, Dion V, Gasser SM. Checkpoint kinases and the INO80 nucleosome remodeling complex enhance global chromatin mobility in response to DNA damage. *Genes Dev* 2013;**27**:1999–2008. https://doi.org/10.1101/gad.222992.113
79. Celona B, Weiner A, Di Felice F *et al.* Substantial histone reduction modulates genomewide nucleosomal occupancy and global transcriptional output. *PLoS Biol* 2011;**9**:e1001086. https://doi.org/10.1371/journal.pbio.1001086
80. Prado F, Cortes-Ledesma F, Aguilera A. The absence of the yeast chromatin assembly factor Asf1 increases genomic instability and sister chromatid exchange. *EMBO Rep* 2004;**5**:497–502. https://doi.org/10.1038/sj.embor.7400128
81. Myung K, Pennaneach V, Kats ES *et al. Saccharomyces cerevisiae* chromatin-assembly factors that act during DNA replication function in the maintenance of genome stability. *Proc Natl Acad Sci USA* 2003;**100**:6640–5. https://doi.org/10.1073/pnas.1232239100
82. Patterton HG, Landel CC, Landsman D *et al.* The biochemical and phenotypic characterization of Hho1p, the putative linker histone H1 of *Saccharomyces cerevisiae*. *J Biol Chem* 1998;**273**:7268–76. https://doi.org/10.1074/jbc.273.13.7268
83. Downs JA, Kosmidou E, Morgan A *et al.* Suppression of homologous recombination by the *Saccharomyces cerevisiae* linker histone. *Mol Cell* 2003;**11**:1685–92. https://doi.org/10.1016/S1097-2765(03)00197-7
84. van Attikum H, Fritsch O, Gasser SM. Distinct roles for SWR1 and INO80 chromatin remodeling complexes at chromosomal double-strand breaks. *EMBO J* 2007;**26**:4113–25. https://doi.org/10.1038/sj.emboj.7601835
85. Kalocsay M, Hiller NJ, Jentsch S. Chromosome-wide Rad51 spreading and SUMO-H2A.Z-dependent chromosome fixation in response to a persistent DNA double-strand break. *Mol Cell* 2009;**33**:335–43. https://doi.org/10.1016/j.molcel.2009.01.016
86. Lademann CA, Renkawitz J, Pfander B *et al.* The INO80 complex removes H2A.Z to promote presynaptic filament formation during homologous recombination. *Cell Rep* 2017;**19**:1294–303. https://doi.org/10.1016/j.celrep.2017.04.051
87. Liu G, Yan J, Wang X *et al.* RPA-mediated recruitment of Bre1 couples histone H2B ubiquitination to DNA replication and repair. *Proc Natl Acad Sci USA* 2021;**118**:e2017497118.
88. Eggler AL, Inman RB, Cox MM. The Rad51-dependent pairing of long DNA substrates is stabilized by replication protein A. *J Biol Chem* 2002;**277**:39280–8. https://doi.org/10.1074/jbc.M204328200
89. Wysocki R, Javaheri A, Allard S *et al.* Role of Dot1-dependent histone H3 methylation in G1 and S phase DNA damage checkpoint functions of Rad9. *Mol Cell Biol* 2005;**25**:8430–43. https://doi.org/10.1128/MCB.25.19.8430-8443.2005
90. Waterman DP, Haber JE, Smolka MB. Checkpoint responses to DNA double-strand breaks. *Annu Rev Biochem* 2020;**89**:103–33. https://doi.org/10.1146/annurev-biochem-011520-104722
91. Chen X, Cui D, Papusha A *et al.* The Fun30 nucleosome remodeller promotes resection of DNA double-strand break ends. *Nature* 2012;**489**:576–80. https://doi.org/10.1038/nature11355
92. Costelloe T, Louge R, Tomimatsu N *et al.* The yeast Fun30 and human SMARCAD1 chromatin remodellers promote DNA end resection. *Nature* 2012;**489**:581–4. https://doi.org/10.1038/nature11353
93. Eapen VV, Sugawara N, Tsabar M *et al.* The *Saccharomyces cerevisiae* chromatin remodeler Fun30 regulates DNA end resection and checkpoint deactivation. *Mol Cell Biol* 2012;**32**:4727–40. https://doi.org/10.1128/MCB.00566-12
94. Bantele SC, Ferreira P, Gritenaite D *et al.* Targeting of the Fun30 nucleosome remodeller by the Dpb11 scaffold facilitates cell cycle-regulated DNA end resection. *eLife* 2017;**6**:e21687. https://doi.org/10.7554/eLife.21687
95. Dibitetto D, Ferrari M, Rawal CC *et al.* Slx4 and Rtt107 control checkpoint signalling and DNA resection at double-strand breaks. *Nucleic Acids Res* 2016;**44**:669–82. https://doi.org/10.1093/nar/gkv1080
96. Ohouo PY, Bastos de Oliveira FM, Liu Y *et al.* DNA-repair scaffolds dampen checkpoint signalling by counteracting the adaptor Rad9. *Nature* 2013;**493**:120–4. https://doi.org/10.1038/nature11658
97. Pfander B, Diffley JF. Dpb11 coordinates Mec1 kinase activation with cell cycle-regulated Rad9 recruitment. *EMBO J* 2011;**30**:4897–907. https://doi.org/10.1038/emboj.2011.345
98. Puddu F, Granata M, Di Nola L *et al.* Phosphorylation of the budding yeast 9–1–1 complex is required for Dpb11 function in the full activation of the UV-induced DNA damage checkpoint. *Mol Cell Biol* 2008;**28**:4782–93. https://doi.org/10.1128/MCB.00330-08
99. Mazon G, Lam AF, Ho CK *et al.* The Rad1–Rad10 nuclease promotes chromosome translocations between dispersed repeats. *Nat Struct Mol Biol* 2012;**19**:964–71. https://doi.org/10.1038/nsmb.2359
100. Kockler ZW, Osia B, Lee R *et al.* Repair of DNA breaks by break-induced replication. *Annu Rev Biochem* 2021;**90**:165–91. https://doi.org/10.1146/annurev-biochem-081420-095551
101. Hung SH, Wong RP, Ulrich HD *et al.* Monoubiquitylation of histone H2B contributes to the bypass of DNA damage during and after DNA replication. *Proc Natl Acad Sci USA* 2017;**114**:E2205–14. https://doi.org/10.1073/pnas.1612633114
102. White CI, Haber JE. Intermediates of recombination during mating type switching in *Saccharomyces cerevisiae*. *EMBO J* 1990;**9**:663–73. https://doi.org/10.1002/j.1460-2075.1990.tb08158.x
103. Wolner B, van Komen S, Sung P *et al.* Recruitment of the recombinational repair machinery to a DNA double-strand break in yeast. *Mol Cell* 2003;**12**:221–32. https://doi.org/10.1016/S1097-2765(03)00242-9
104. Sugawara N, Wang X, Haber JE. *In vivo* roles of Rad52, Rad54, and Rad55 proteins in Rad51-mediated recombination. *Mol Cell* 2003;**12**:209–19. https://doi.org/10.1016/S1097-2765(03)00269-7
105. Mason JM, Chan YL, Weichselbaum RW *et al.* Non-enzymatic roles of human RAD51 at stalled replication forks. *Nat Commun* 2019;**10**:4410. https://doi.org/10.1038/s41467-019-12297-0
106. Trujillo KM, Osley MA. A role for H2B ubiquitylation in DNA replication. *Mol Cell* 2012;**48**:734–46. https://doi.org/10.1016/j.molcel.2012.09.019
107. Lin CY, Wu MY, Gay S *et al.* H2B mono-ubiquitylation facilitates fork stalling and recovery during replication stress by coordinating Rad53 activation and chromatin assembly. *PLoS Genet* 2014;**10**:e1004667. https://doi.org/10.1371/journal.pgen.1004667

108. Liu G, Li J, He B *et al.* Bre1/RNF20 promotes Rad51-mediated strand exchange and antagonizes the Srs2/FBH1 helicases. *Nat Commun* 2023;**14**:3024. https://doi.org/10.1038/s41467-023-38617-z
109. Lo CSY, van Toorn M, Gaggioli V *et al.* SMARCAD1-mediated active replication fork stability maintains genome integrity. *Sci Adv* 2021;**7**:eabe7804. https://doi.org/10.1126/sciadv.abe7804
110. Lewis TS, Sokolova V, Jung H *et al.* Structural basis of chromatin regulation by histone variant H2A.Z. *Nucleic Acids Res* 2021;**49**:11379–91. https://doi.org/10.1093/nar/gkab907
111. Segala G, Bennesch MA, Pandey DP *et al.* Monoubiquitination of histone H2B blocks eviction of histone variant H2A.Z from inducible enhancers. *Mol Cell* 2016;**64**:334–46. https://doi.org/10.1016/j.molcel.2016.08.034
112. Wojcik F, Dann GP, Beh LY *et al.* Functional crosstalk between histone H2B ubiquitylation and H2A modifications and variants. *Nat Commun* 2018;**9**:1394. https://doi.org/10.1038/s41467-018-03895-5
113. Awad S, Ryan D, Prochasson P *et al.* The Snf2 homolog Fun30 acts as a homodimeric ATP-dependent chromatin-remodeling enzyme. *J Biol Chem* 2010;**285**:9477–84. https://doi.org/10.1074/jbc.M109.082149
114. Flaus A, Martin DM, Barton GJ *et al.* Identification of multiple distinct Snf2 subfamilies with conserved structural motifs. *Nucleic Acids Res* 2006;**34**:2887–905. https://doi.org/10.1093/nar/gkl295
115. Krogan NJ, Keogh MC, Datta N *et al.* A Snf2 family ATPase complex required for recruitment of the histone H2A variant Htz1. *Mol Cell* 2003;**12**:1565–76. https://doi.org/10.1016/S1097-2765(03)00497-0
116. Durand-Dubief M, Will WR, Petrini E *et al.* SWI/SNF-like chromatin remodeling factor Fun30 supports point centromere function in *S.cerevisiae*. *PLoS Genet* 2012;**8**:e1002974. https://doi.org/10.1371/journal.pgen.1002974
117. Ferrari M, Rawal CC, Lodovichi S *et al.* Rad9/53BP1 promotes DNA repair via crossover recombination by limiting the Sgs1 and Mph1 helicases. *Nat Commun* 2020;**11**:3181. https://doi.org/10.1038/s41467-020-16997-w
118. Sanford EJ, Comstock WJ, Faca VM *et al.* Phosphoproteomics reveals a distinctive Mec1/ATR signaling response upon DNA end hyper-resection. *EMBO J* 2021;**40**:e104566. https://doi.org/10.15252/embj.2020104566
119. Xie B, Sanford EJ, Hung SH *et al.* Multi-step control of homologous recombination via Mec1/ATR suppresses chromosomal rearrangements. *EMBO J* 2024;**43**:3027–43. https://doi.org/10.1038/s44318-024-00139-9
120. Vasan S, Deem A, Ramakrishnan S *et al.* Cascades of genetic instability resulting from compromised break-induced replication. *PLoS Genet* 2014;**10**:e1004119. https://doi.org/10.1371/journal.pgen.1004119
121. Briggs SD, Xiao T, Sun ZW *et al.* Gene silencing: trans-histone regulatory pathway in chromatin. *Nature* 2002;**418**:498. https://doi.org/10.1038/nature00970
122. Steger DJ, Lefterova MI, Ying L *et al.* DOT1L/KMT4 recruitment and H3K79 methylation are ubiquitously coupled with gene transcription in mammalian cells. *Mol Cell Biol* 2008;**28**:2825–39. https://doi.org/10.1128/MCB.02076-07
123. Huyen Y, Zgheib O, Ditullio RA *et al.* Methylated lysine 79 of histone H3 targets 53BP1 to DNA double-strand breaks. *Nature* 2004;**432**:406–11. https://doi.org/10.1038/nature03114
124. Bantele SCS, Pfander B. Nucleosome remodeling by Fun30(SMARCAD1) in the DNA damage response. *Front Mol Biosci* 2019;**6**:78. https://doi.org/10.3389/fmolb.2019.00078
125. Densham RM, Garvin AJ, Stone HR *et al.* Human BRCA1–BARD1 ubiquitin ligase activity counteracts chromatin barriers to DNA resection. *Nat Struct Mol Biol* 2016;**23**:647–55. https://doi.org/10.1038/nsmb.3236
126. Mehta A, Beach A, Haber JE. Homology requirements and competition between gene conversion and break-induced replication during double-strand break repair. *Mol Cell* 2017;**65**:515–26. https://doi.org/10.1016/j.molcel.2016.12.003
127. Boltengagen M, Verhagen D, Wolff MR *et al.* A single fiber view of the nucleosome organization in eukaryotic chromatin. *Nucleic Acids Res* 2024;**52**:166–85. https://doi.org/10.1093/nar/gkad1098

Received: September 12, 2024. **Revised:** January 21, 2025. **Editorial Decision:** January 22, 2025. **Accepted:** January 29, 2025